HHS Public Access

Author manuscript

Nature. Author manuscript; available in PMC 2017 November 20.

Published in final edited form as:

Nature. 2017 May 18; 545(7654): 365–369. doi:10.1038/nature22344.

TRAF2 and OTUD7B govern a ubiquitin-dependent switch that regulates mTORC2 signalling

Bin Wang[1,2,*], **Zuliang Jie**[3,*], **Donghyun Joo**[3], **Alban Ordureau**[4], **Pengda Liu**[2], **Wenjian Gan**[2], **Jianping Guo**[2], **Jinfang Zhang**[2], **Brian J. North**[2], **Xiangpeng Dai**[2], **Xuhong Cheng**[3], **Xiuwu Bian**[5], **Lingqiang Zhang**[6], **J. Wade Harper**[4], **Shao-Cong Sun**[3], and **Wenyi Wei**[2]

[1]Department of Gastroenterology, Institute of Surgery Research, Daping Hospital, Third Military Medical University, Chongqing 400042, China

[2]Department of Pathology, Beth Israel Deaconess Medical Center, Harvard Medical School, Boston, Massachusetts 02215, USA

[3]Department of Immunology, The University of Texas MD Anderson Cancer Center, 7455 Fannin Street, Box 902, Houston, Texas 77030, USA

[4]Department of Cell Biology, Harvard Medical School, Boston, Massachusetts 02115, USA

[5]Institute of Pathology and Southwest Cancer Center and Key Laboratory of Tumor Immunopathology, Ministry of Education of China, Southwest Hospital, Third Military Medical University, Chongqing 400038, China

[6]State Key Laboratory of Proteomics, Beijing Proteome Research Center, Beijing Institute of Radiation Medicine, Collaborative Innovation Center for Cancer Medicine, Beijing 100850, China

Abstract

The mechanistic target of rapamycin (mTOR) has a key role in the integration of various physiological stimuli to regulate several cell growth and metabolic pathways[1]. mTOR primarily functions as a catalytic subunit in two structurally related but functionally distinct multi-component kinase complexes, mTOR complex 1 (mTORCl) and mTORC2 (refs [1, 2]). Dysregulation of mTOR signalling is associated with a variety of human diseases, including

Correspondence and requests for materials should be addressed to W.W. (wwei2@bidmc.harvard. edu) or S.-C.S. (ssun@mdanderson.org).

*These authors contributed equally to this work.

Online Content Methods, along with any additional Extended Data display Items and Source Data, are available in the online version of the paper; references unique to these sections appear only in the online paper.

Supplementary Information is available in the online version of the paper.

Author Contributions B.W., Z.J., PL., S.-C.S. and W.W. designed the research. B.W., Z.J., A.O., D.J., P.L., W.G., J.G., J.Z., B.J.N., X.D. and X.C. performed experiments and/or analysed data. S.-C.S. and W.W. supervised the study. X.B., L.Z. and J.W.H. provided critical reagents. B.W., Z.J., PL., S.-C.S. and W.W. interpreted data and wrote the manuscript. All authors commented on the manuscript.

The authors declare no competing financial interests. Readers are welcome to comment on the online version of the paper.

Publisher's note: Springer Nature remains neutral with regard to jurisdictional claims in published maps and institutional affiliations.

Reviewer Information *Nature* thanks D. Fruman and the other anonymous reviewer(s) for their contribution to the peer review of this work.

metabolic disorders and cancer[1]. Thus, both mTORCl and mTORC2 kinase activity is tightly controlled in cells. mTORCl is activated by both nutrients[3–6] and growth factors[7], whereas mTORC2 responds primarily to extracellular cues such as growth-factor-triggered activation of PI3K signalling[8–10]. Although both mTOR and GβL (also known as MLST8) assemble into mTORC1 and mTORC2 (refs [11–15]), it remains largely unclear what drives the dynamic assembly of these two functionally distinct complexes. Here we show, in humans and mice, that the K63-linked polyubiquitination status of GβL dictates the homeostasis of mTORC2 formation and activation. Mechanistically, the TRAF2 E3 ubiquitin ligase promotes K63-linked polyubiquitination of GβL, which disrupts its interaction with the unique mTORC2 component SIN1 (refs [12–14]) to favour mTORC1 formation. By contrast, the OTUD7B deubiquitinase removes polyubiquitin chains from GβL to promote GβL interaction with SIN1, facilitating mTORC2 formation in response to various growth signals. Moreover, loss of critical ubiquitination residues in GβL, by either K305R/K313R mutations or a melanoma-associated GβL(ΔW297) truncation, leads to elevated mTORC2 formation, which facilitates tumorigenesis, in part by activating AKT oncogenic signalling. In support of a physiologically pivotal role for OTUD7B in the activation of mTORC2/AKT signalling, genetic deletion of *Otud7b* in mice suppresses Akt activation and *Kras*-driven lung tumorigenesis *in vivo*. Collectively, our study reveals a GβL-ubiquitination-dependent switch that fine-tunes the dynamic organization and activation of the mTORC2 kinase under both physiological and pathological conditions.

Protein ubiquitination controls protein stability, trafficking and protein-protein interactions via eight possible linkages of polyubiquitin chains[16,17]. Although K63-linked ubiquitination of mTOR[18] and Rag GTPase[19,20] regulates mTORCl activity, it remains unclear whether the ubiquitin pathway governs mTORC2 activation or the homeostasis of mTOR complexes. We observed that among all core mTOR complex components, only GβL and to a lesser extent RPTOR, were heavily ubiquitinated in cells (Fig. 1a). Ubiquitination of GβL, but not RPTOR, was markedly reduced upon stimulation with growth factors (Fig. 1b and Extended Data Fig. 1a–e). Moreover, reduced GβL ubiquitination by acute insulin (5–30 min) or epidermal growth factor (8–24 min) stimulation at early time points correlated with elevated GβL interaction with mTORC2 components SIN1 and RICTOR, and reduced binding to mTORC1 component RPTOR (Fig. 1c, d and Extended Data Fig. 1f–l). Therefore, GβL ubiquitination status may have a physiological role in regulating mTOR complex homeostasis.

Notably, ubiquitinated GβL under serum-starved conditions was primarily K63-linked, the levels of which were significantly reduced upon insulin stimulation (Fig. 1e–g, Extended Data Fig. 1m, n), indicating a novel role for K63-linked ubiquitination of GβL in modulating mTOR complex homeostasis. Among several E3 ligases capable of catalysing K63-linked ubiquitination, only TRAF2 specifically interacted with GβL and promoted GβL ubiquitination (Extended Data Fig. 2a–f). GβL ubiquitination was significantly reduced in *Traf2*$^{-/-}$ *cells* or cells expressing mutant TRAF2 with its RING domain removed (Extended Data Fig. 2g–i). Moreover, TRAF2 promoted non-proteolytic K63-linked ubiquitination of GβL, without affecting its protein stability in a manner dependent on the TRAF2 recognition motif (Fig. 1h and Extended Data Fig. 2j–n).

Furthermore, the dynamic fluctuation of GβL ubiquitination in wild-type mouse embryonic fibroblasts (MEFs) upon growth factor stimulation was largely abolished in *Traf2*$^{-/-}$ MEFs, accompanied by elevated Akt(phosphorylated (p)S473) and Akt(pS473)-dependent phosphorylation of Foxo1 (ref. [12, 13, 15]), but minimal changes in Akt(pT308) or S6k(pT389) (Fig. 1i, j and Extended Data Fig. 2o, p). Under normal culture conditions, manipulation of TRAF2 also impacted primarily on AKT(pS473) levels, but minimally on S6K(pT389) or AKT ubiquitination (Fig. 1k and Extended Data Fig. 2q, r). Moreover, GβL ubiquitination was unresponsive to mTOR inhibition or TNFα stimulation (Extended Data Fig. 2s, t). Thus, loss of TRAF2-mediated GβL ubiquitination largely facilitates the activation of mTORC2, with minimal effects on mTORC1 or PDK1 signalling.

To elucidate further the molecular mechanisms underlying TRAF2-mediated ubiquitination of GβL in regulating mTORC2 complex organization and activity, we found that the seventh WD40 motif (WD7) in GβL was both necessary and sufficient for GβL ubiquitination in cells (Fig. 2a, b). Furthermore, WD7 mediated the specific interaction of GβL with SIN1 (ref. [12–14]), a unique component of mTORC2, while the adjacent WD6 motif mediated the specific GβL interaction with RPTOR (ref. 11), the mTORC1-specific subunit (Fig. 2c and Extended Data Fig. 3a–c). Given that mTORC2-, but not mTORC1-associated GβL was poorly ubiquitinated (Extended Data Fig. 3d–f), we reasoned that GβL ubiquitination on the WD7 motif by TRAF2 may regulate GβL distribution into mTOR complexes. Indeed, depletion of *Traf2* elevated mT ORC2 complex formation, but reduced mTORC1 abundance. Conversely, ectopic expression of TRAF2 enhanced mTORCl formation coupled with impaired mTORC2 assembly (Fig. 2d and Extended Data Fig. 3g–j).

Next we sought to identify the critical GβL ubiquitination sites within WD7, and found that mutating the two conserved lysine residues, K305 and K313, drastically reduced GβL ubiquitination levels (Extended Data Fig. 4a–c). Consistently, CRISPR-mediated introduction of the KRKR mutations into the endogenous *MLST8* gene (GβL(KRKR)) significantly reduced GβL K63-linked ubiquitination in cells, which subsequently enhanced mTORC2 assembly coupled with reduced mTORCl formation, a phenotype observed upon depleting *Traf2* or deleting the TRAF2 binding site in GβL (Fig. 2e, f and Extended Data Fig. 4d–i).

Moreover, TRAF2 suppressed mTORC2 complex formation and mTORC2/AKT signalling in part by increasing GβL ubiquitination (Fig. 2g and Extended Data Fig. 4j, k). As a result, under physiological conditions such as growth factor stimulation, compared to cells expressing wild-type GβL, cells expressing GβL(KRKR) displayed enhanced GβL interaction with mTORC2 components to activate mTORC2/Akt signalling, but exhibited reduced GβL interaction with Rptor and slightly affected S6k(pT389) levels at later time points (Fig. 2h and Extended Data Fig. 4l, m).

Hence, GβL ubiquitination may provide a molecular switch to govern the balance between mTORC2 and mTORCl (Fig. 2i). In doing so, TRAF2-mediated GβL ubiquitination on K305/K313 in the WD7 domain precludes SIN1 or RICTOR binding, thereby disrupting mTORC2 complex integrity, thus indirectly favouring RPTOR binding on the adjacent WD6 motif to promote mTORCl complex formation. However, upon insulin stimulation, loss of

GβL WD7 ubiquitination allows interaction between GβL and SIN1, thereby priming a population of non-ubiquitinated GβL to be incorporated into mTORC2, which fine-tunes the dynamic balance of mTOR complexes for optimal response to upstream signalling cues. Importantly, consistent with a previous study[15], GβL is indispensable for mTORC2, but not mTORCl, integrity and activation (Extended Data Fig. 5a), while the underlying mechanism remains not fully understood[2,15]. However, reduced GβL integration into mTORCl at early time points of growth stimulation or in cells depleted of *Traf2* or expressing GβL(KRKR) might be compensated by elevated mTORCl kinase activity, possibly due to increased phosphorylation of TSC2 by Akt to reduce TSC2 inhibition of mTORCl[21] (Figs 1j, 2h and Extended Data Figs 4l, m and 5b).

Notably, reintroducing ubiquitination and SINl-binding deficient GβL(ΔWD7) into *MLST8*-depleted cells failed to restore AKT(pS473) to confer chemoresistance and transforming capacities (Extended Data Fig. 6a–e). More importantly, compared to wild-type cells, cells expressing the ubiquitination-deficient GβL mutants (GβL(PEAA) and GβL(KRKR)) displayed elevated AKT(pS473), coupled with increased chemoresistance, colony formation, anchorage-independent growth and tumour growth, while inhibiting AKT activity reversed these malignant phenotypes (Fig. 3a–e and Extended Data Fig. 6f–v). These data suggest that loss of GβL-ubiquitination-mediated promotion of mTORC2 complex formation is physiologically critical for activation of mTORC2/AKT oncogenic signalling, contributing to cellular chemoresistance and tumorigenicity.

In keeping with a possible role of loss of GβL ubiquitination in favouring human cancers through elevated mTORC2 signalling[9,10,22], a GβL(ΔW297) mutant missing GβL ubiquitination sites (K305 and K313) was identified in melanoma (Fig. 3f, sample ID: TCGA-FS-A1ZZ-06). GβL(Δ W297) was poorly ubiquitinated in cells, leading to an elevated formation of mTORC2 complex and increased mTORC2 activity towards phosphorylating S473 of AKT (Fig. 3g—i and Extended Data Fig. 7a–d). Consequently, GβL(ΔW297)-expressing cells displayed enhanced chemoresistance and tumorigenicity, while inhibiting AKT activity attenuated these malignant behaviours (Fig. 3j, k and Extended Data Fig. 7e–m). Thus, the oncogenic activity of GβL(ΔW297) may be partially due to loss of GβL-ubiquitination-mediated disruption of mTOR complex homeostasis and aberrant AKT activation.

We went on to identify the potential deubiquitinase(s) (DUBs) that removes ubiquitin chains from GβL. To this end, a subset of the ovarian tumour (OTU) family of DUBs has demonstrated specificity towards hydrolysing the K63-linkage[23]. Notably, OTUD7B, but no other OTU DUB family members examined, specifically interacted with GβL to remove GβL ubiquitination in cells (Fig. 4a and Extended Data Fig. 8a, b). Moreover, OTUD7B reduced the levels of K63-, but not K48-linked GβL ubiquitination, minimally affecting the half-life of GβL protein (Fig. 4b, Extended Data Fig. 8c–f). Additionally, OTUD7B, but not UCH-L1, a DUB for RPTOR[24], targeted GβL for deubiquitination (Extended Data Fig. 8g–j). Thus OTUD7B, apart from hydrolysing K11 ubiquitin chains[23,25,26], is also a bona fide DUB that removes K63-linkage polyubiquitination from GβL.

In keeping with a role for GβL ubiquitination in dictating mTORC2 homeostasis, deletion of *Otud7b* reduced mTORC2, but elevated mTORC1 formation, leading to impaired activation of mTORC2/Akt signalling (Fig. 4c, d and Extended Data Fig. 8k, l). Deletion of *Otud7b* did not significantly affect Akt ubiquitination, but largely abolished the decrease of GβL ubiquitination in cells induced by growth factor stimulation (Fig. 4e and Extended Data Fig. 8m, n). Consequently, elevated mTORC2 and an inverse reduction in mTORC1 complex formation at early time points (5–30 min) of growth factor stimulation in wild-type cells was largely impaired in $Otud7b^{-/-}$ MEFs, leading to attenuated Akt(pS473) levels with a minimal increase in S6k(pT389) (Fig. 4e and Extended Data Fig. 8n–q). Biologically, attenuated AKT(pS473) by *OTUD7B* deletion subsequently led to chemosensitization and reduced transforming capacities (Extended Data Fig. 8r–u). Hence, OTUD7B mediates removal of polyubiquitination from GβL to promote mTORC2 formation and activation of downstream AKT signalling.

Consistently, upon growth factor stimulation, the reduction of GβL ubiquitination was attenuated upon *OTUD7B* knockdown (Extended Data Fig. 9a, b). Reduced GβL ubiquitination was largely due to induced binding of OTUD7B to GβL, but not loss of TRAF2 binding (Fig. 4f and Extended Data Fig. 9c–e). On the other hand, the interaction of UCHL1 and RPTOR was minimally affected by growth factor signalling (Extended Data Fig. 9f). These results indicate that OTUD7B-mediated deubiquitination, rather than TRAF2-induced ubiquitination is physiologically regulated by growth factor signalling to control GβL ubiquitination and mTOR complex homeostasis.

Moreover, polyubiquitin chains on GβL are required for its interaction with OTUD7B, largely via the ubiquitin-associated (UBA) domain on OTUD7B, leading to GβL deubiquitination and downstream mTORC2/AKT signalling (Extended Data Fig. 9g–n). In support of this notion, OTUD7B facilitated GβL integration into mTORC2, probably through deubiquitinating GβL, to elevate AKT(pS473), thereby facilitating chemoresistance and cell growth (Extended Data Fig. 9o–t). OTUD7B-mediated cleavage of K63-linked polyubiquitin chains on GβL appears to be a common mechanism to promote mTORC2/AKT signalling, as knockdown of *OTUD7B* downregulated AKT(pS473) and conferred chemosensitivity to cancer cells with elevated mTORC2/AKT signalling due to oncogenic events such as *PTEN* deletion, *PIK3CA, EGFR* or *KRAS* mutations (Extended Data Fig. 10a–d). Consistently, the *OTUD7B* gene was frequently amplified in various cancers including lung cancers, where high OTUD7B mRNA levels in lung cancers correlated with lower survival probability in a cohort of 1,926 patients (Extended Data Fig. 10e, f).

Given that binding of p110α subunit to Ras and subsequent activation of PI3K is required for the development and maintenance of *Kras*-driven lung tumours[27,28], we further assessed whether Otud7b-promoted mTORC2/Akt signalling is causally related to *Kras*-induced lung tumorigenesis. In the $Otud7b^{+/+}$ background, $Kras^{LA2}$ mice developed spontaneous lung tumour nodules at the age of 16–23 weeks (Fig. 4g). Notably, $Otud7b^{+/-}$ $Kras^{LA2}$ mice developed lung tumours at comparable levels to $Otud7b^{+/+}$ $Kras^{LA2}$ mice. Conversely, homozygous *Otud7b* deletion markedly reduced lung tumour burden induced by $Kras^{LA2}$ (Fig. 4g–i and Extended Data Fig. 10g). Compared with $Otud7b^{+/+}$ $Kras^{LA2}$ mice,

Otud7b$^{-/-}$ *Kras*^{LA2} counterparts formed about 50% less tumour nodules and the tumour size was profoundly reduced. Consequently, *Otud7b*$^{-/-}$ *Kras*^{LA2} mice had a significantly higher survival probability than *Otud7b*$^{+/+}$ *Kras*^{LA2} mice (Fig. 4j), probably due to reduced tumour burden, since *Otud7b*$^{-/-}$ and *Otud7b*$^{+/+}$ mice were comparable in survival without *Kras*^{LA2} activation[29]. Furthermore, Akt(pS473) was reduced in *Otud7b*$^{-/-}$ tumours and normal lung tissues, as compared to the *Otud7b*$^{+/+}$ littermates (Fig. 4k). These results suggest that Otud7b is required for *Kras*-driven lung tumour initiation and progression at least partially by facilitating activation of mTORC2/Akt signalling.

Collectively, these results reveal a GβL polyubiquitination-dependent mechanism governing the integrity of mTORC2. These findings also reveal new regulatory roles of OTUD7B and TRAF2, essential regulators of the NF-κB pathway[29], in mTORC2/AKT signalling and cancer biology, in addition to a reported role of OTUD7B in enhancing breast cancer proliferation[30]. Importantly, OTUD7B, rather than TRAF2, appears to be the primary regulatory mechanism to translate growth signals via active cleavage of the K63 polyubiquitin chain on GβL, thereby modulating mTORC2 homeostasis under physiological conditions (Fig. 4l). Pathologically, OTUD7B-mediated activation of mTORC2/AKT signalling may be a critical molecular event down-stream of the RAS/PI3K pathway to favour *Kras*^{LA2}-driven lung tumorigenesis, suggesting that OTUD7B may be a potential therapeutic target against diseases harbouring hyperactivated PI3K/mTOR signalling such as cancer.

METHODS

Cell culture and transfection

Human embryonic kidney 293 (HEK293) cells, HEK293FT, OVCAR5, A375, HeLa, and mouse embryonic fibroblasts (MEFs) were maintained in Dulbecco's Modified Eagle's Medium (DMEM) containing 10% fetal bovine serum (FBS), 100 units of penicillin and 100 mg ml^{-1} streptomycin. *Gβl*$^{+/+}$ and *Gβ*$^{-/-}$ MEFs were generous gifts from D. M. Sabatini (Whitehead Institute for Biomedical Research, Massachusetts Institute of Technology). *Traf2*$^{+/+}$ and *Traf2*$^{-/-}$ MEFs were obtained from Y. Sun (Department of Radiation Oncology, University of Michigan). *Otud7b*$^{+/+}$ and *Otud7b*$^{-/-}$ MEFs have been described previously[29]. All the cell lines were routinely tested negative for mycoplasma contamination. Transfection was performed using lipofectamine 2000 reagent as described previously[9,10].

For serum starvation, 32 h post-transfection, cells were washed with PBS twice and cultured in FBS-free DMEM for 14–16 h. To initiate growth factor signalling, the medium was added with EGF (Sigma E9644, 100 ng ml^{-1}) or insulin (Invitrogen 41400–045,100 nM) for indicated period of times.

Antibodies

Rabbit polyclonal antibody against human OTUD7B was purchased from Cell Signaling Technology (CST). Anti-mouse Otud7b antibody was obtained from Proteintech. Anti-SIN1 antibodies were purchased from CST (12860) or generated (K87) in the B. Su laboratory (Department of Immunobiology and the Vascular Biology and Therapeutics Program, Yale

University). Primary antibodies against TRAF2 (4724), RICTOR (9476), RPTOR (2280), mTOR (2983), AKT (pS473) (4051 and 4060), AKT(pT308) (2965), S6K(pT389) (9205), pFOX-O1(Thr24)/FOXO3a(Thr32) (9464), AKT (4691), S6K (2708), FOXO1 (9454), GST tag (2625) and Myc Tag (2278 and 2276) were purchased from CST. Primary antibodies against GβL were purchased from CST (3274) and Bethyl (A300-679A). Rabbit polyclonal anti-HA antibody (MMS-101P) was purchased from BioLegend. Mouse monoclonal anti-HA antibody (sc-805) was obtained from Santa Cruz. Rabbit antibody against the Flag epitope (F7425), mouse monoclonal anti-Flag antibody (F3165), mouse monoclonal anti-Flag M2 affinity agarose beads (A2220), mouse monoclonal anti-HA agarose beads (A2095), anti-tubulin antibody (T5168), peroxidase-conjugated secondary anti-mouse (A4416) and anti-rabbit (A4914) antibodies were purchased from Sigma. These primary antibodies were used at a 1:1,000 dilution and secondary antibodies were diluted at 1:3,000 in 5% non-fat milk for immunoblotting analysis. For immunoblot analysis of mouse normal lung and tumour tissues, antibodies for Akt1 (B-1), HSP60 (H1) were purchased from Santa Cruz Biotechnology, Inc.

Plasmids and shRNAs

Expression vectors CMV-GST-GβL (amino acid (aa) 1–326), CMV-GST-GβL-ΔWD6 (deleting aa 211–262), CMV-GST-GβL-Δ WD7 (aa 1–271), CMV-GST-GβL-WD6 (aa 211–271), CMV-GST-GβL-WD7 (aa 263–326), CMV-GST-GβL-WD6+7 (aa 211–326) and CMV-GST-UCH-L1 were generated by subcloning the corresponding cDNAs into the pCMV-GST vector via BamHI/BglII and XhoI/SalI sites. HA-GβL (aa 1–326), HA-GβL-Δ WD6 (deleting aa 211–262), HA-GβL-ΔWD7 (aa 1–271), HA-GβL-ΔWD6+7 (aa 1–211), HA-GβL-ΔW297 (aa 1–297), HA-SIN1, HA-RICTOR, HA-Rptor, HA-mTOR, HA-TRAF1, HA-TRAF2 and HA-TRAF3 were constructed by cloning the corresponding cDNAs into pcDNA3-HA vector via BamHI and XhoI sites. Flag-TRAF2 and Flag-TRAF2-ΔRING were kindly gifted by Y. Sun (Department of Radiation Oncology, University of Michigan). Myc-RPTOR, Myc-TRAF2, Myc-TRAF6 or Flag-TRAF6, Flag-SKP2, Flag-RNF168 and Flag-SIN1 were constructed by cloning the corresponding cDNAs into pcDNA3-Myc or pcDNA3-Flag vector via BamHI and XhoI sites. Flag-Myc-OTUB1, Flag-Myc-OTUB2, Flag-Myc-OTUD3, Flag-Myc-OTUD4, Flag-Myc-OTUD5, Flag-Myc-OTUD6A, Flag-Myc-OTUD6B, Flag-Myc-OTUD7A and Flag-Myc-OTUD7B constructs have been described previously[31]. The HA-GβL(K305R), HA-GβL (K313R), HA-GβL(K305R/K313R) (KRKR), HA-GβL(P265A/E267A) (PEAA), Flag-Myc-OTUD7B(C194A) mutants[29,32] were constructed using the Site-Directed Mutagenesis Kit (Stratagene) following the manufacturer's instructions. His-Ub, His-Ub(K6R), His-Ub(K11R), His-Ub(K27R), His-Ub(K29R), His-Ub(K33R), His-Ub(K48R), His-Ub(K63R), His-Ub(K0), His-Ub(K48) only and His-Ub(K63) only vectors were provided by P. P. Pandolfi (Beth Israel Deaconess Medical Center, Harvard Medical School). GβL shRNA vectors were purchased from GE Healthcare Dharmacon (Clone ID: TRCN0000039758, TRCN0000039759, TRCN0000039760, TRCN0000039761, TRCN0000039762). Lentiviral shRNA vectors depleting human *OTUD7B* were from an shRNA library targeting human de-ubiquitinating enzymes (OBS Catalogue number: RHS6054), purchased from Thermo Scientific Open Biosystems. The target sequences are *OTUD7B* shRNA #1: 5′-

CGGCGGAAGGAGAAGTCAA-3′ and *OTUD7B* shRNA #2: 5′-ACGTCTTTGTCCTTGCTCA-3′.

Virus packaging and cell infection

For lentiviral shRNA infection, HEK293FT cells were transfected with shGFP or GβL shRNA or OTUD7B shRNA plenti-puro vectors, together with packing vectors (A8.9 and VSVG plasmids) using lipofectamine 2000 reagent as previously described[9,10]. To restore GβL expression, GβL mutants resistant to shRNA (GβL-shRes) were constructed from HA-GβL, HA-GβL(PEAA) and HA-GβL(KRKR) vectors using the following primer sets: 5′-CAATAGCACCGGCAACTGCTACGTATGGAATCTGACG-3′ (sense) and 5′-CGTCAGATTCCATACGTAGCAGTTGCCGGTGCTATTG-3′ (antisense). The shRes HA-GβL, HA-GβL(PEAA) and HA-GβL(KRKR) were subcloned into pBabe-hygro retroviral vectors[33] and co-transfected with packaging vectors (Retro-VSVG, JK3, and CMV-TAT plasmids) into HEK293FT cells using lipofectamine 2000 reagent. All the constructs were confirmed by DNA sequencing. The cells were infected with various virus particles and selected with medium containing puromycin and/or hygromycin for at least three days.

Ubiquitination assays in cells

Cellular ubiquitination assays were performed as described previously[34]. In brief, HEK293 cells were co-transfected with His-Ub and the indicated vectors for 48 h and lysed in denaturing condition (buffer A: 6 M guanidine-HCl, 0.1 M $Na_2HPO_4/Na_2H_2PO_4$, 10 mM imidazole (pH 8.0)). After sonication, the poly-ubiquitinated proteins were purified by incubation with nickel-nitrilotriacetic acid (Ni-NTA) matrices (QIAGEN) for 3 h at room temperature. Histidine pull-down products were washed sequentially once in buffer A, twice in buffer A/TI mixture (buffer A:buffer TI = 1:3), and once in buffer TI (25 mM Tris-HCl and 20 mM imidazole (pH 6.8)). The poly-ubiquitinated proteins were separated by SDS-PAGE for immunoblot analysis.

UB-AQUA/PRM proteomics

HEK293 cells were transfected with CMV-GST-GβL and ubiquitin expression constructs. Thirty-two hours post-transfection, the cells were serum starved for 16 h, with or without insulin stimulation, and lysed using Triton buffer for GST pull-down. The GST pull-down products were eluted with glutathione-containing buffer and then subjected to Ubiquitin Absolute Quantification (UB-AQUA) mass spectrometry (MS) analysis of ubiquitin chain linkage. For UB-AQUA/PRM, samples were subject to TCA precipitation. Samples were digested first with Lys-C (in 100 mM tetraethylammonium bromide (TEAB), 0.1% Rapigest (Waters Corporation), 10% (vollvol) acetonitrile (ACN)) for 2 h at 37 °C, followed by the addition of trypsin and further digested overnight. Digests were acidified with an equal volume of 5% (vollvol) formic acid (FA) to a pH of approximately 2 for 30 min, dried down, and resuspended in 1% (vollvol) FA.

UB-AQUA/PRM was performed largely as described previously but with several modifications[35–37]. A collection of 16 heavy-labelled reference peptides[36], each containing a single $^{13}C/^{15}N$-labelled amino acid, was produced at Cell Signaling Technologies and quantified by amino acid analysis. UB-AQUA peptides from working stocks (in 5% (vol/vol)

FA) were diluted into the digested sample (in 1% (vol/vol) FA) to be analysed to an optimal final concentration predetermined for individual peptide. Samples and AQUA peptides were oxidized with 0.05% hydrogen peroxide for 20 min, subjected to C18 StageTip and resuspended in 1% (vol/vol) FA. MS data were collected sequentially by liquid chromatography (LC)lMS on a Q Exactive mass spectrometer (Thermo Fisher Scientific) coupled with a Famos Autosampler (LC Packings) and an Accela600 LC pump (Thermo Fisher Scientific). Peptides were separated on a 100 μm i.d. microcapillary column packed with around 0.5 cm of Magic C4 resin (5 μm, 100 Å; Michrom Bioresources) followed by approximately 20 cm of Accucore C18 resin (2.6 μm, 150 Å; Thermo Fisher Scientific). Peptides were separated using a 45 min gradient of 3–25% ACN in 0.125% FA with a flow rate of about 300 nl min^{-1}. The scan sequence began with an Orbitrap full MS1 spectrum with the following parameters: resolution of 70,000, scan range of 200–1,000 Thomson (Th), AGC target of1×10^6, maximum injection time of 250 ms, and profile spectrum data type. This scan was followed by 12 targeted MS2 scans selected from a scheduled inclusion list with a 8-min retention time window. Each targeted MS2 scan consisted of high-energy collision dissociation (HCD) with the following parameters: resolution of 17,500, AGC of 1×10^5, maximum injection time of 200 ms, isolation window of 1 Th, normalized collision energy (NCE) of 23, and profile spectrum data type. Raw files were searched, and precursor and fragment ions were quantified using Skyline version 3.5 (ref. 38). Data generated from Skyline were exported into an Excel spreadsheet for further analysis as previously described[36]. Total UB was determined as the average of the total UB calculated for each individual locus, unless specified otherwise.

Mass spectrometry analysis

Samples were subjected to reduction (10 mM TCEP) and alkylation (20 mM chloroacetamide) followed by TCA precipitation. Samples were digested overnight at 37 °C with Lys-C and trypsin (in 100 mM TEAB, 0.1% Rapigest, 10% (vol/vol) acetonitrile (ACN)). Digests were acidified with an equal volume of 5% (vol/vol) formic acid (FA) to a pH of approximately 2 for 30 min, dried down, resuspended in 1% (vol/vol) FA before C18 StageTip (packed with Empore C18; 3M Corporation) desalting. Eluted peptide were resuspended in 1% FA and mass spectrometry data were collected using a Qexactive mass spectrometer (Thermo Fisher Scientific, San Jose, CA) with a Famos Autosampler (LC Packings) and an Accela600 liquid chromatography (LC) pump (Thermo Fisher Scientific). Peptides were separated on a 100 μm inner diameter microcapillary column packed with around 0.5 cm of Magic C4 resin (5 μm, 100 Å, Michrom Bioresources) followed by about 20 cm of Accucore C18 resin (2.6 μm, 150 Å, Thermo Fisher Scientific). Peptides were separated using an 80 min gradient of 3 to 35% acetonitrile in 0.125% formic acid with a flow rate of approximately 300 nl min^{-1}. The scan sequence began with an MS1 spectrum (Orbitrap analysis; resolution 70,000; mass range 300–1,500 m/z; automatic gain control (AGC) target 1×10^6; maximum injection time 250 ms). Precursors for MS2 analysis were selected using a Top20 most abundant peptides. MS2 analysis consisted of high-energy collision-induced dissociation (quadrupole ion trap analysis; AGC 1×10^5; normalized collision energy (NCE) 25; maximum injection time 60 ms; resolution 17,500). Sequest-based identification using a Human UNIPROT database followed by a target decoy-based linear discriminant analysis was used for peptide and protein identification as described[39].

Parameters used for database searching include: 50 p.p.m. Precursor mass tolerance; 0.03 Da product ion mass tolerance; tryptic digestion with up to three missed cleavages; carboxyamidomethylation of Cys was set as a fixed modification, while oxidation of Met was set as variable modifications. Localization of diGly sites used a modified version of the A-score algorithm as described[40,41]. A-scores of 13 were considered localized.

Generation of the *GβL*^{KRKR} knock-in cell line by CRISPR-Cas9 technology

The *GβL*^{KRKR} knock-in cell line was generated following the protocol described previously[42]. The sgRNA (5′-TCCAGCTTCCTCGGACAACC-3′) targeting the genomic sequence close to the GβL K305/K313 site was designed using the CRISPR design tool (http://crispr.mit.edu) and cloned into GeneArt CRISPR nuclease vector with OFP reporter (Life Technologies, A21174). A 167-nt single-stranded oligodeoxynucleotides (ssODNs) was used as the template with KRKR mutation and a silent change to the PAM site that do not alter the amino acid sequence. The sgRNA construct and the ssODNs were co-transfected into HEK293 cells. Forty-eight hours post-transfection, the OFP-positive cells were enriched by FACS sorting and seeded into a 96-well plate with one cell per well. The genomic DNA of individual clone was extracted using the Quick Extract DNA Extraction Solution (Epicentre, Q09050) and used as the template to amplify the DNA fragment containing the K305/K313 site. The PCR products were cut by BspEI (NEB, R0540L) to screen the potential correct clones. Finally, knock-in mutations were verified by the Sanger sequencing method. The primers for amplification of the genomic DNA were: forward, 5′-GCAGCTTCCCCTCTGCTG-3′; reverse, 5′-AGGGGAGGGTCTGCTCTG-3′. ssODNs: 5′-GCACCAGGCAGTCCCGAGGGGTCACAGGCTAGCCCAGCACACTGTCATTGAAGGCCAGGCAGACAACAGCCCGCTGGTGGCCGCCATACTCTCTCCGGATCTCTCCAGTCTCCACACACCAGAGCCGGGCGAGGTTGTCCGAGGAAGCTGGAGGGGGAGATTGTGCA-3′.

Protein half-life assays

To measure the half-life of GβL protein in cells, a cycloheximide (CHX)-based assay was performed following our previously described experimental procedures[34].

Gel-filtration chromatography assays

Traf2$^{-/-}$ MEFs, *GβL*^{KRKR} knock-in HEK293 cells, *Otud7b*$^{-/-}$ MEFs, and corresponding wild-type cells, or *GβL*-depleted A375 cells stably expressing GβL or GβL(ΔW297) were cultured in serum-containing medium were washed with phosphate-buffered saline, lysed in 0.5 ml of CHAPS buffer supplemented with protease inhibitors (Complete Mini, Roche) and phosphatase inhibitors (phosphatase inhibitor cocktail set I and II, Calbiochem). Alternatively, HEK293 cells were serum starved for 16 h and stimulated with or without insulin (100 nM) for 15 min, and lysed using CHAPS buffer. The gel filtration chromatography assays were performed as described previously[9]. In brief, whole-cell lysates (WCL) were filtered through a 0.45 μm syringe filter and protein concentration was adjusted to 8 mg ml^{-1} with CHAPS buffer. Afterward, 500 μl of the WCL was injected onto a Superdex 200 10/300 GL column (GE Lifesciences cat. no. 17-5175-01). Chromatography was performed on the AKTA-FPLC (GE Lifesciences cat. no. 18-1900-26) with CHAPS

buffer. One column volume of eluates was fractionated with 500 μl in each fraction, at the elution speed of 0.3 ml min^{-1}. Aliquots (25 μl each) of each fraction were resolved by SDS-PAGE gels and detected with indicated antibodies.

Immunoblots and immunoprecipitation

CHAPS buffer (40 mM Tris, pH 7.5, 120 mM NaCl, 1 mM EDTA, 0.3% CHAPS)[11,43], Triton buffer (40 mM Tris, pH 7.5, 120 mM NaCl, 1 mM EDTA, 1% Triton X-100) or EBC buffer (50 mM Tris, pH 7.5, 120 mM NaCl, 0.5% NP-40) was added with protease inhibitors (Complete Mini, Roche) and phosphatase inhibitors (cocktail set I and II, Calbiochem). When analysing mTOR complex formation, cells were lysed using CHAPS buffer to preserve mTOR complex integrity. Under other experimental conditions, WCL were collected using EBC, CHAPS or Triton buffer as indicated. Protein concentrations were measured using Bio-Rad protein assay kit in a spectrophotometer (Beckman Coulter DU-800). To perform immunoprecipitation, same amounts of WCL were incubated with the primary antibodies (1–2 μg) for 4 h at 4 °C. The incubation tubes were added with Protein A/G sepharose beads (GE Healthcare) to incubate for 1 h and washed four times with NETN buffer (20 mM Tris, pH 8.0, 100 mM NaCl, 1 mM EDTA, 0.5% NP-40) or CHAPS buffer. For western blot analysis, equal amounts of WCL or immunoprecipitate were separated by SDS-PAGE and immunoblotted with indicated antibodies.

Cell viability assays

To examine cell viability, cells were seeded at 3,000 per well in 96-well plates overnight and treated with DMEM medium containing indicated doses of etoposide (Sigma, E1383) or cisplatin (Selleck S1166) for 24 h. The viability was measured using a CellTiter-Glo Luminescent Cell Viability Assay Kit (Promega), following the manufacturer's instructions.

Colony formation assays

The indicated tumour cells were plated in six-well plates (300 or 600 cells per well) and maintained for up to 10–12 days. Visible colonies were washed with PBS and fixed with 10% acetic acid/10% methanol for 30 min, and then stained with 0.4% crystal violet/20% ethanol. After washing with distilled water and air-dried, the colonies were quantified and analysed.

Soft agar assays

The anchorage-independent growth capacity of tumour cells was examined by soft agar assays, as described previously[9,10]. In brief, each well of six-well plates was coated with the bottom layer noble agar (0.8%). The single tumour cells were seeded into the top layer medium containing 0.4% agar. Specifically, 3×10^4 OVCAR5 cells or 1×10^4 A375 cells were plated in the top layer of each well. The wells were added with 500 μl complete DMEM medium every 3 days. Four weeks later, the cells were stained with iodonitrotetrazolium chloride and visible colonies were counted. The assays were performed in triplicates.

Xenograft assays in nude mice

All animal experiments were approved by the Beth Israel Deaconess Medical Center IACUC Committee review board. *GβL*-depleted OVCAR5 cells stably expressing HA-GβL or HA-GβL(KRKR) were mixed with matrigel (1:1) and inoculated into the flank of female nude mice (2.5×10^6 cells per injection, 6 mice for each group). Alternatively, *GβL*-depleted A375 cells stably expressing HA-GβL or HA-GβL(ΔW297) were injected subcutaneously into female nude mice (5×10^6 cells per mice and 7 mice for each cell line). After tumour establishment, the palpable xenograft nodules were measured for the longest diameter (L) and the shortest diameter (W) every three days using a calliper. The tumour volumes were calculated with the formula: $L \times W^2 \times 0.5$. After indicated days, the mice were killed humanely. None of the xenograft tumours reached the maximal tumour volume permitted by the institutional IACUC Committee. The xenograft tumours were dissected and weighted.

Genetic knockout mouse models

Otud7b$^{-/-}$ mice were generated in B6.129sv genetic background and subsequently backcrossed for four generations to the C57BL/6 background[29]. *Kras*^{LA2} mice (in B6.129s2 background) were described previously[44] and provided by the NCI Mouse Repository. The *Kras*^{LA2} mice develop tumours in the lung as a result of spontaneous recombination that generates the oncogenic *Kras* mutant *Kras*^{G12D}. *Otud7b*$^{+/-}$ heterozygous mice were crossed with *Kras*^{LA2} mice to generate age-matched *Otud7b*$^{+/+}$*Kras*^{LA2} and *Otud7b*$^{-/-}$ *Kras*^{LA2} mice for experiments. Mice were maintained in specific-pathogen-free facility of the University of Texas MD Anderson Cancer Center, and the experiments were performed according to the Institutional Animal Care and Use Committee.

Analysis of lung tumour development in mice

Age-matched *Otud7b*$^{+/+}$*Kras*^{LA2} and *Otud7b*$^{-/-}$*Kras*^{LA2} mice killed humanely at the indicated ages for analyses of lung tumours. Following perfusion with PBS, the lungs were removed and fixed in 10% phosphate-buffered formalin (pH 7.4) for histology analyses. For the survival study, *Otud7b*$^{+/+}$ and *Otud7b*$^{-/-}$ mice with *Kras*^{G12D} were housed in the animal core facility and the monitored every three days for the indicated time period to calculate survival rate. Haematoxylin and eosin (H&E)-stained lung tissue slides were analysed for tumour numbers and size. Total tissue lysates from the lung or dissected tumours were also prepared and subjected to IB assays.

Survival analysis of lung cancer patients

Kaplan-Meier survival curves were generated using the Kaplan-Meier Plotter website for lung cancer (Version 2015, http://kmplot.com)[45] and statistical significance was determined by the log-rank test. Gene expression and patient survival data were downloaded from public databases including Gene Expression Omnibus (GEO), European Genome-Phenome Archive (EGA), and The Cancer Genome Atlas (TCGA).

Statistics

The majority of experiments were repeated at least three times to obtain data for indicated statistical analyses. No statistical method was used to calculate sample size. Group variation

was not estimated before experiments. The experiments were not randomized in the animal studies and investigators were not blind during experiments and outcome assessment. For western blotting data, representative images from 3–5 biological replicate experiments were shown. For quantification analysis, the original western blot images were quantified using ImageJ software to measure the intensity of some key blots for statistical analysis. The number of mice per group was described in the corresponding figure legends and none of the animals was excluded from the experiment. All quantitative data were presented as mean ± s.d. Results were analysed by a two-tailed unpaired or paired Student's *t*-test or two-way ANOVA, as appropriate. $*P < 0.05$; $**P < 0.01$; $***P < 0.001$. For survival analysis, the Kaplan-Meier survival curves were compared using the log-rank test.

Data availability

Uncropped images for immunoblots are provided in Supplementary Fig. 1. Mouse model data are also provided in the Source Data. All other relevant data are available from the corresponding author upon reasonable request.

Extended Data

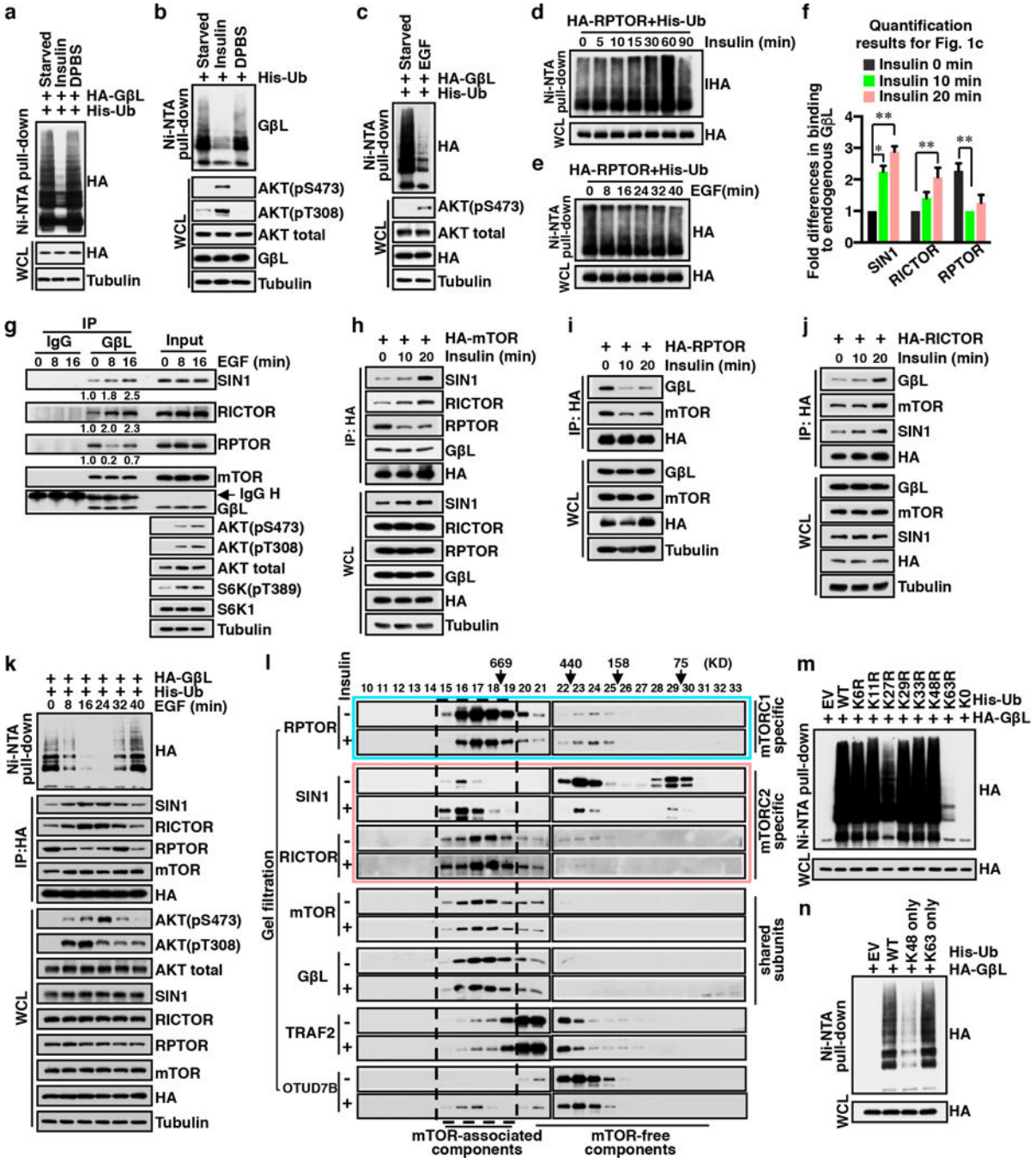

Extended Data Figure 1. The polyubiquitination status of GβL and mTORC2 kinase formation is regulated by upstream physiological stimuli

a–c, The polyubiquitination status of GβL is reduced in response to growth factor stimulation. Immunoblot (IB) analysis of whole-cell lysates (WCL) or Ni-NTA pull-down products under denaturing conditions derived from HEK293 cells transfected with His-Ub together with (**a, c**) or without (**b**) HA-GβL vector. Cells were serum starved for 16 h and treated with insulin (100 nM) or Dulbecco's phosphate-buffered saline (DPBS) for 30 min

(**a, c**), or EGF (100 ng ml^{-1}) for 16 min (**b**) before harvesting. **d, e**, Unlike GβL, polyubiquitination of RPTOR is minimally affected by growth signalling induction. IB analysis of WCL or Ni-NTA pull-down products under denaturing conditions derived from HEK293 cells transfected with HA-RPTOR and His-Ub constructs. Thirty-two hours post-transfection, cells were subjected to serum starvation for 16 h, and then exposed to insulin (100 nM) (**d**) or EGF (100 ng ml^{-1}) (**e**) at indicated time points before harvesting. f, Quantification results from three independent experiments showing fold differences of endogenous GβL binding to SIN1, RICTOR and Rptor in cells in response to insulin stimulation, as indicted in Fig. 1c. Data are mean ± s.d. The intensity of each blot generated using ImageJ software were analysed by twotailed paired Student's *t*-test, $*P < 0.05$, $**P < 0.01$. **g**, The assembly of endogenous mTORC1 and mTORC2 responds to physiological growth factor stimulation. IB analysis of GβL immunoprecipitate or WCL derived from HEK293 cells serum starved for 16 h, then stimulated with EGF (100 ng ml^{-1}), and lysed at indicated time points using CHAPS buffer for immunoprecipitation and IB analysis. Rabbit IgG antibody was used as negative control for GβL immunoprecipitation. For quantification analysis, levels were arbitrarily set at 1.0 at the 0 min time point. **h**–**j**, Growth factor stimulation enhances mTORC2, but inhibits mTORC1 formation at early time points. IB analysis of HA immunoprecipitate or WCL derived from HEK293 cells transfected with HA-mTOR (**h**), HA-RPTOR (i), or HA-RICTOR (**j**) constructs. Thirty-two hours post-transfection, cells were serum starved for 16 h, then stimulated with insulin (100 nM), and lysed at indicated time points using CHAPS buffer for immunoprecipitation and IB analysis. k, Polyubiquitination of GβL inversely correlates with mTORC2 integrity and activity in response to EGF stimulation. IB analysis of WCL or Ni-NTA pull-down products under denaturing conditions derived from HEK293 cells transfected with HA-GβL and His-Ub constructs. Thirty-two hours post-transfection, cells were subjected to serum starvation for 16 h, then treated with EGF (100 ng ml^{-1}) for indicated time points, lysed for HA immunoprecipitation or His pull-down assays and IB analysis. l, Transient insulin stimulation increases the relative abundance of endogenous mTORC2, but reduces mTORC1 formation in cells. HEK293 cells were subjected to serum starvation for 16 h and treated with or without insulin (100 nM) for 15 min, and lysed using CHAPS buffer. WCL was filtered and run through an FPLC Superdex 200 column. Five hundred microlitres of elute was collected for each fraction and a 1/20 volume of each fraction was resolved on SDS-PAGE and subjected to IB analysis. **m**, GβL polyubiquitination linkage was examined by transfecting His-tagged wild-type (WT) and indicated KR ubiquitin mutants together with HA-GβL into HEK293 cells, followed by IB analysis of Ni-NTA pull-down products and WCL. **n**, Polyubiquitination of GβL could largely be detected in cells transfected with wild-type ubiquitin and lysine-63-only ubiquitin (K63 only), but not lysine-48-only ubiquitin mutant (K48 only) constructs. IB analysis of Ni-NTA pull-down products and WCL derived from HEK293 cells transfected with HA-GβL and wild-type His-Ub or mutant constructs as indicated. For uncropped gels, see Supplementary Fig. 1.

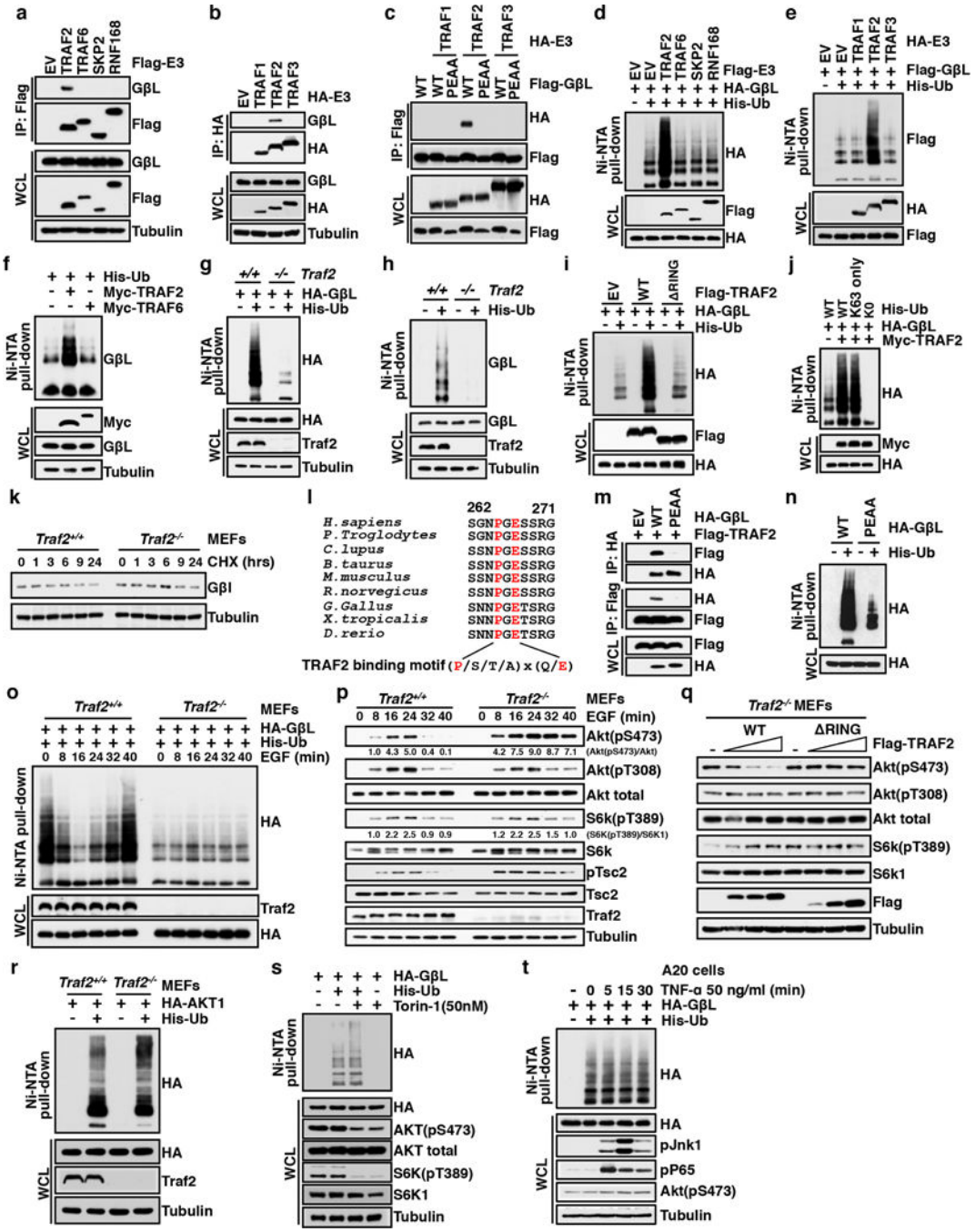

Extended Data Figure 2. The TRAF2 E3 ligase catalyses K63-linked polyubiquitination of GβL and inhibits the activity of mTORC2 kinase in cells

a–c, GβL specifically interacts with TRAF2 in cells. IB analysis of immunoprecipitate and WCL derived from HEK293 cells transfected with indicated constructs. **d, e**, Polyubiquitination of GβL in HEK293 cells was examined by transfecting GβL, various indicated E3 ligases and His-Ub constructs, followed by IB analysis of WCL and Ni-NTA pull-down products under denaturing conditions. **f**, TRAF2, but not TRAF6, promotes polyubiquitination of endogenous GβL in cells. IB analysis of WCL or Ni-NTA pull-down

products under denaturing conditions derived from HEK293 cells transfected indicated constructs. **g, h**, Genetic deletion of *Traf2* attenuates polyubiquitination of GβL in cells. IB analysis of WCL or Ni-NTA pull-down products under denaturing conditions derived from $Traf2^{+/+}$ and $Traf2^{-/-}$ MEFs that were transfected with (**g**) or without (**f**) HA-GβL, along with His-Ub vector. i, TRAF2 promotes polyubiquitination of GβL in an E3 ligase activity-dependent manner. IB analysis of WCL or Ni-NTA pull-down products under denaturing conditions derived from $Traf2^{-/-}$ MEFs transfected with HA-GβL and His-Ub, along with wild-type or the activity-deficient TRAF2 (ΔRING) mutant construct. j, TRAF2 promotes K63-linked polyubiquitination of GβL in cells. IB analysis of WCL or Ni-NTA pull-down products under denaturing conditions derived from HEK293 cells transfected with HA-GβL and His-Ub construct, or His-tagged ubiquitin mutants containing only lysine 63 (K63 only) or no lysine residue (K0). **k**, Genetic deletion of *Traf2* does not affect the half-life of endogenous GβL protein in cells. IB analysis of WCL derived from $Traf2^{+/+}$ and $Traf2^{-/-}$ MEFs treated with 100 μg ml^{-1} cycloheximide (CHX) for indicated time points before harvesting. **l**, A schematic diagram showing the evolutionarily conserved consensus TRAF2-binding motif within GβL. **m**, Mutating the TRAF2 consensus motif abolishes GβL binding to TRAF2 in cells. IB analysis of WCL and immunoprecipitate from HEK293 cells transfected with TRAF2, together with GβL or GβL(PEAA) constructs. **n**, Mutating the TRAF2 consensus motif largely abolishes GβL polyubiquitination in cells. Polyubiquitination status of GβL in HEK293 cells was examined by transfecting HA-tagged GβL or GβL(PEAA) with His-Ub constructs, followed by IB analysis of WCL and Ni-NTA pull-down products under denaturing conditions. **o**, Genetic deletion of *Traf2* attenuates polyubiquitination of GβL in cells. IB analysis of WCL or Ni-NTA pull-down products under denaturing conditions derived from $Traf2^{+/+}$ and $Traf2^{-/-}$ MEFs transfected with HA-GβL and His-Ub. Thirty-two hours post-transfection, cells were subjected to serum starvation for 16 h and exposed to EGF (100 ng ml^{-1}) for indicated time points before harvesting. **p**, Loss of *Traf2* leads to elevated Akt phosphorylation in response to EGF. IB analysis of WCL derived from $Traf2^{+/+}$ and $Traf2^{-/-}$ MEFs that were subjected to serum starvation for 16 h and treated with EGF (100 ng ml^{-1}) for indicated time points before harvesting. For quantification analysis, levels are normalized to total Akt or S6k1, respectively, and arbitrarily set at 1.0 at the 8 min time point of $Traf2^{+/+}$ MEFs. **q**, TRAF2 inhibits Akt(pSer473) in an E3 ligase activity-dependent manner. IB analysis of WCL derived from $Traf2^{-/-}$ MEFs transfected with Flag-tagged wild-type TRAF2 or the activity-deficient TRAF2(ΔRING) constructs. **r**, Genetic deletion of *Traf2* minimally affects Akt ubiquitination in cells. IB analysis of WCL or Ni-NTA pull-down products under denaturing conditions derived from $Traf2^{+/+}$ and $Traf2^{-/-}$ MEFs transfected with HA-Akt1 and His-Ub. **s**, Inhibition of mTOR kinase activity does not significantly affect polyubiquitination of GβL in cells. IB analysis of WCL or Ni-NTA pulldown products under denaturing conditions derived from $Traf2^{-/-}$ MEFs transfected with HA-GβL and His-Ub constructs. Thirty-two hours post-transfection, cells were treated with or without Torin-1 (50 nM) for 6 h before harvesting. **t**, Activation of TNF receptor signalling does not significantly regulate polyubiquitination of GβL in cells. IB analysis of WCL or Ni-NTA pull-down products under denaturing conditions derived from mouse B cell lymphoma cell line A20 cells that were transfected with HA-GβL and His-Ub constructs. Thirty-two hours post-transfection,

cells were treated with or without TNFα (50 ng ml^{-1}) for indicated time points before harvesting. For uncropped gels, see Supplementary Fig. 1.

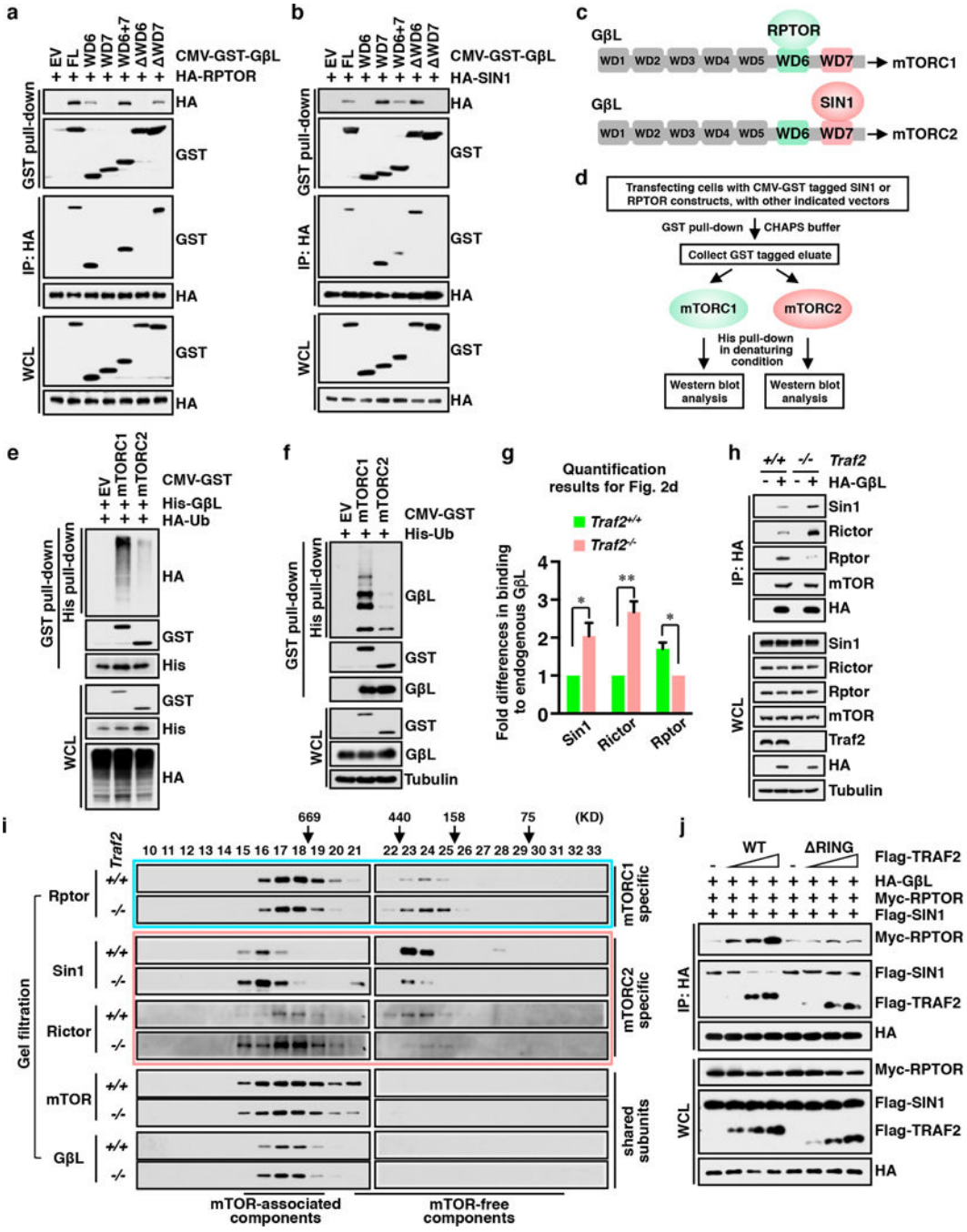

Extended Data Figure 3. TRAF2 promotes polyubiquitination of GβL at the WD7 motif, a specific SIN1-interacting domain, to impair the assembly of mTORC2 kinase

a, b, GβL utilizes different WD40 motifs to interact with the two distinct mTOR complexes. Specifically, the WD6 motif is the major GβL domain interacting with the unique mTORCl subunit, RPTOR, while the WD7 motif primarily binds a mTORC2-specific subunit, SIN1 in cells. IB analysis of WCL and GST pull-down products derived from HEK293 cells

transfected with HA-RPTOR (**a**) or HA-SIN1 (**b**) constructs, together with indicated GST-GβL mammalian expression vectors. **c**, A schematic illustration showing specific binding of RPTOR to the WD6 domain of GβL to be incorporated into mTORCl, and binding of SIN1 to the WD7 motif of GβL to promote mTORC2 formation. **d**, A schematic model showing the experimental procedures of a sequential pull-down assay, which is performed to detect the existence of GβL ubiquitin moieties in either GST-purified mTORCl or mTORC2. **e**, Detection of ubiquitinated GβL species in GST-purified mTORCl, but not mTORC2. HEK293 cells were transfected with either GST-SIN1 or GST-Rptor expression constructs, together with His-GβL and HA-Ub vectors. Forty-eight hours post-transfection, cells were harvested in CHAPS buffer to specifically pull down the intact mTORC1 or mTORC2 from cell lysates with GST-conjugated beads. The GST pull-down products were eluted using glutathione (GSH)-containing buffer and the elutes were subjected to second round of His pull-down assays in denaturing condition. Afterwards, the resulting samples were resolved on SDS-PAGE and subjected to IB analysis to detect the ubiquitination status of mTORC1- and mTORC2-associated GβL, respectively. **f**, GβL is largely ubiquitinated in GST-purified mTORC1, but not mTORC2. HEK293 cells were transfected with either GST-SIN1 or GST-Rptor constructs, together with His-Ub vector. Following a similar protocol as described in **e**, His pull-down products and WCL were subjected to IB analysis of GβL ubiquitin moieties in either mTORC1 or mTORC2. **g**, Quantification results from three independent experiments showing fold differences of endogenous GβL binding to Sin1, Rictor and Rptor in *Traf2*$^{+/+}$ and *Traf2*$^{-/-}$ MEFs, as indicated in Fig. 2d (mean ± s.d., *P< 0.05, **P< 0.01, paired Student's t-test). **h**, IB analysis of WCL and HA immunoprecipitate derived from *Traf2*$^{+/+}$ and *Traf2*$^{-/-}$ MEFs transfected with HA-GβL or empty vector (EV) as a negative control. **i**, Deletion of *Traf2* increases the formation of endogenous mTORC2, meanwhile reduces endogenous mTORC1 formation. *Traf2*$^{+/+}$ and *Traf2*$^{-/-}$ MEFs in normal culture medium were lysed using CHAPS buffer. WCL was fractionated through an FPLC Superdex 200 column. Five hundred microlitres of eluate was collected for each fraction and a 1/20 volume of each fraction was resolved on SDS-PAGE for IB analysis. **j**, TRAF2 promotes GβL interaction with RPTOR, but inhibits GβL-SIN1 binding in an E3-ligase-activity-dependent manner. IB analysis of WCL and HA immunoprecipitate derived from HEK293 cells transfected with HA-GβL, Myc-RPTOR, Flag-SIN1, together with increasing doses of wild-type TRAF2 or the activity-deficient TRAF2(ΔRING) mutant construct. For uncropped gels, see Supplementary Fig. 1.

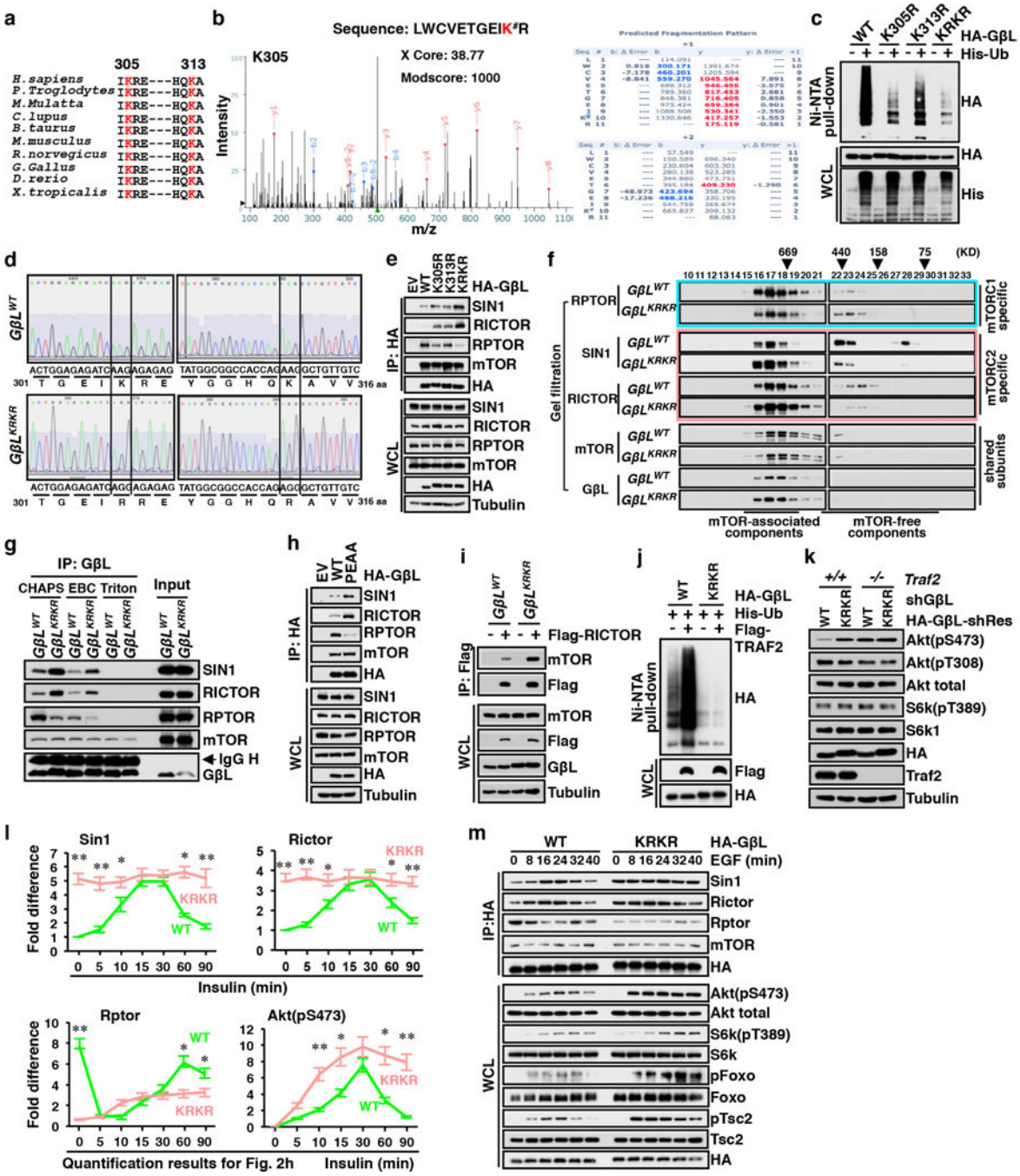

Extended Data Figure 4. Deficiency in GβL ubiquitination at K305/K313 of the WD7 domain promotes mTORC2 formation and kinase activity in cells

a, A schematic diagram showing two evolutionarily conserved lysine residues (K305 and K313) within the WD7 domain of GβL. **b**, Mass spectrometry analysis to identify K305 as one of the major GβL ubiquitination residues within the WD7 domain of GβL in cells. HEK293 cells were transfected with CMV-GST-GβL and ubiquitin expression constructs. Forty-eight hours post-transfection, cells were lysed using Triton buffer for GST pull down. The GST pull-down products were eluted with GSH-containing buffer and then subjected to

mass spectrometry analysis of ubiquitination sites. The recovered GβL peptide and the ubiquitination site (K305) were highlighted in red. **c**, Mutating key lysine residues within the WD7 domain of GβL abolishes GβL ubiquitination in cells. Polyubiquitination of GβL in HEK293 cells was examined by transfecting the indicated HA-GβL constructs with His-Ub, followed by IB analysis of WCL and Ni-NTA pull-down products under denaturing conditions. **d**, Sequencing of PCR products from genomic DNA demonstrates the introduction of A to G substitution at the codon encoding K305 and K313 of GβL gene in a $G\beta L^{KRKR}$ knock-in HEK293 cell line generated by CRISPR-mediated gene editing. **e**, Loss of GβL ubiquitination leads to elevated GβL binding to mTORC2 components, and reduced GβL binding to mTORCl components in cells. IB analysis of WCL and HA immunoprecipitate derived from HEK293 cells transfected with indicated GβL plasmids. **f**, $G\beta L^{KRKR}$ knock-in cells, compared to wild-type cells, display an increased formation of endogenous mTORC2 and a reduced formation of endogenous mTORCl. HEK293 cells harbouring wild-type GβL, or ubiquitination-deficient $G\beta L^{KRKR}$ were lysed using CHAPS buffer. The WCL was run through an FPLC Superdex 200 column to collect fractionated cell eluates. A 1/20 volume of each fraction was subjected to IB analysis. **g**, Loss of ubiquitination of endogenous GβL promotes mTORC2 formation in CHAPS and EBC buffer, but not Triton buffer. IB analysis of GβL immunoprecipitate derived from $G\beta L^{KRKR}$ knock-in or wild-type HEK293 cells lysed using indicated buffers for immunoprecipitation. The resulting samples were resolved on SDS-PAGE for IB analysis. IB result of WCL prepared using Triton buffer were shown as input. **h**, Mutating the specific TRAF2 binding site in GβL promotes GβL integration into mTORC2, but inhibits its integration into mTORC1. IB analysis of WCL and HA immunoprecipitate derived from HEK293 cells transfected with HA-GβL or the TRAF2-non-interacting GβL(PEAA) mutant construct. **i**, Loss of ubiquitination of endogenous GβL promotes RICTOR interaction with mTOR to form mTORC2. IB analysis of WCL or Flag immunoprecipitate derived from $G\beta L^{KRKR}$ knock-in or wild-type HEK293 cells transfected with Flag-RICTOR construct. Forty-eight hours post-transfection, cells were lysed using CHAPS buffer for Flag immunoprecipitation. The resulting samples were resolved on SDS-PAGE for IB analysis. **j**, TRAF2 promotes polyubiquitination of GβL, but not the GβL(KRKR) mutant, in cells. IB analysis of WCL or Ni-NTA pull-down products under denaturing conditions derived from HEK293 cells transfected with Flag-TRAF2 and His-Ub, along with HA-GβL, or HA-GβL(KRKR) mutant constructs. k, Compared to ectopic expression of wild-type GβL, reintroducing GβL(KRKR) into *GβL*-depleted $Traf2^{+/+}$ cells significantly elevated Akt(pS473). Conversely, in *G/3L-depleted* $Traf2^{-/-}$ cells, reintroducing GβL(KRKR) did not result in any detectable elevation of Akt(pS473). The $Traf2^{-/-}$ MEFs and wild-type MEFs were depleted of endogenous GβL using lentirivus-medicated delivery of short hairpin RNAs (shRNAs) targeting GβL and then reintroduced with GβL and GβL(KRKR) using pBabe-retroviral expression system. The kinase activity of mTORC2/Akt oncogenic signalling in these stable cell lines was analysed by IB analysis of WCL. **l**, Quantification results for fold differences of GβL binding to Sin 1, Rictor and Rptor, or the Akt(pS473) levels, in $G\beta l^{-/-}$ MEFs stably expressing GβL or the GβL(KRKR) mutant at the indicated time points of insulin stimulation, as indicated in Fig. 2h. Data from three independent experiments were presented as mean ± s.d. The intensity of each blot generated using ImageJ software were analysed by paired Student's *t*-test, $*P < 0.05$, $**P < 0.01$. **m**, GβL polyubiquitination status dictates the dynamic assembly of mTOR

complexes in response to EGF stimulation. As such, deficiency in GβL polyubiquitination results in elevated mTORC2 formation and elevated downstream Akt activation. IB analysis of WCL and HA immunoprecipitate derived from Gβl$^{-/-}$ MEFs stably expressing HA-GβL or the ubiquitination-deficient HA-GβL(KRKR) mutant that were generated by retroviral infection, followed by serum starvation for 16 h and exposure to EGF (100 ng ml^{-1}) before harvesting using CHAPS buffer. For uncropped gels, see Supplementary Fig. 1.

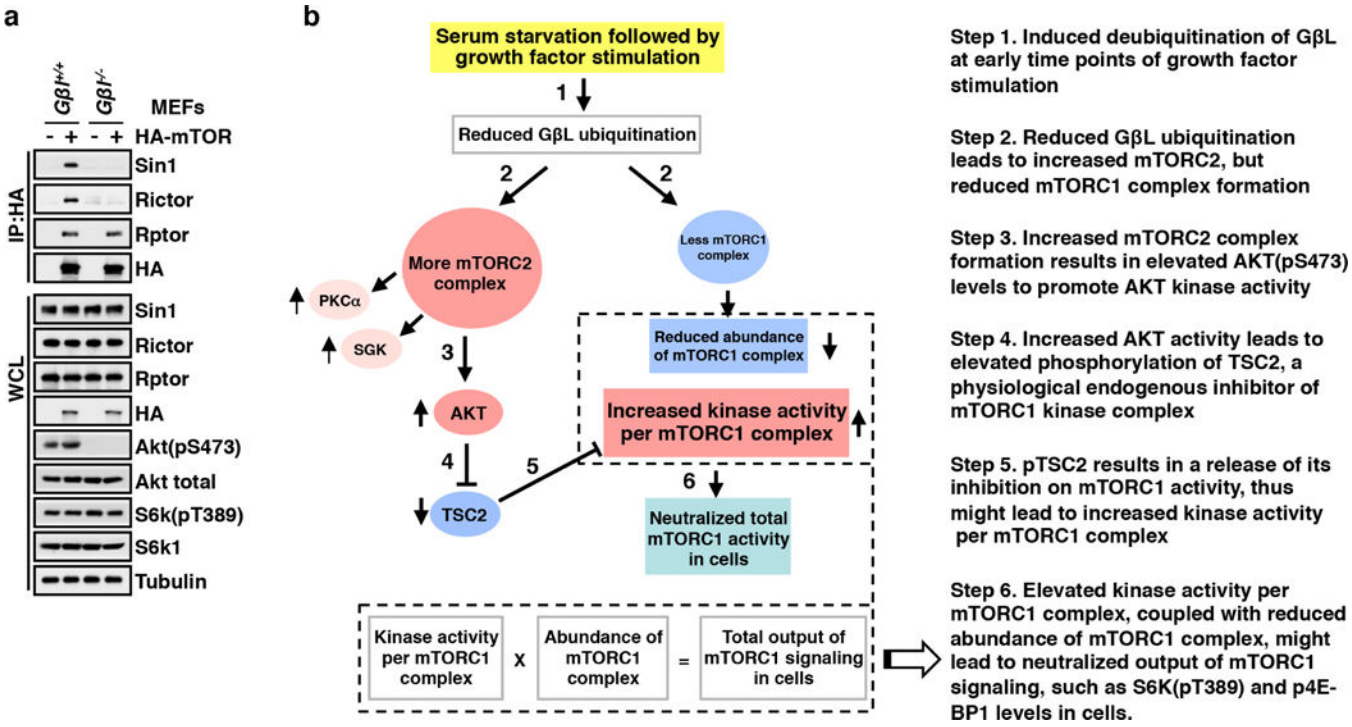

Extended Data Figure 5. A schematic model depicting the neutralized regulatory effect of reduced GβL ubiquitination on the total output of mTORC1 signalling in cells

a, Consistent with a previous study, deletion of *Gβl* impairs the integrity and kinase activity of mTORC2, but not mTORC1, in mouse embryonic fibroblasts (MEFs) derived from *Gβl*$^{+/+}$ and *Gβl*$^{-/-}$ embryos. *Gβl*$^{+/+}$ and *Gβl*$^{-/-}$ MEFs were transfected with HA-mTOR plasmid, with empty vector as a control. Forty-eight hours post-transfection, cells were lysed using CHAPS buffer for HA immunoprecipitation and IB analysis. **b**, The schematic illustration of a proposed neutralization model to elucidate the possible underlying mechanism that the observed reduction of mTORC1 abundance resulting from a decrease of GβL ubiquitination in either *Traf2*$^{-/-}$ cells, *GβL*^{KRKR}*-expressing* cells, or at early time points of growth factor stimulation, might be compensated by elevated kinase activity per mTORC1, thus leading to neutralized output of mTORC1 signalling in these cells. This compensation effect is largely derived from reduced GβL ubiquitination-induced elevation of mTORC2 kinase formation that will eventually lead to an increase in AKT-mediated phosphorylation of TSC2, a physiological endogenous inhibitor of mTORC1 signalling that functions largely as a GAP for Rheb. Phosphorylation of TSC2 at multiple sites by AKT releases TSC2 inhibitory effects towards mTORC1, which might further lead to an elevated kinase activity per mTORC1 to balance off its reduction in mTORC1 abundance, thereby

leading to minimal perturbation on the total output of mTORC1 signalling in these cells. For uncropped gels, see Supplementary Fig. 1.

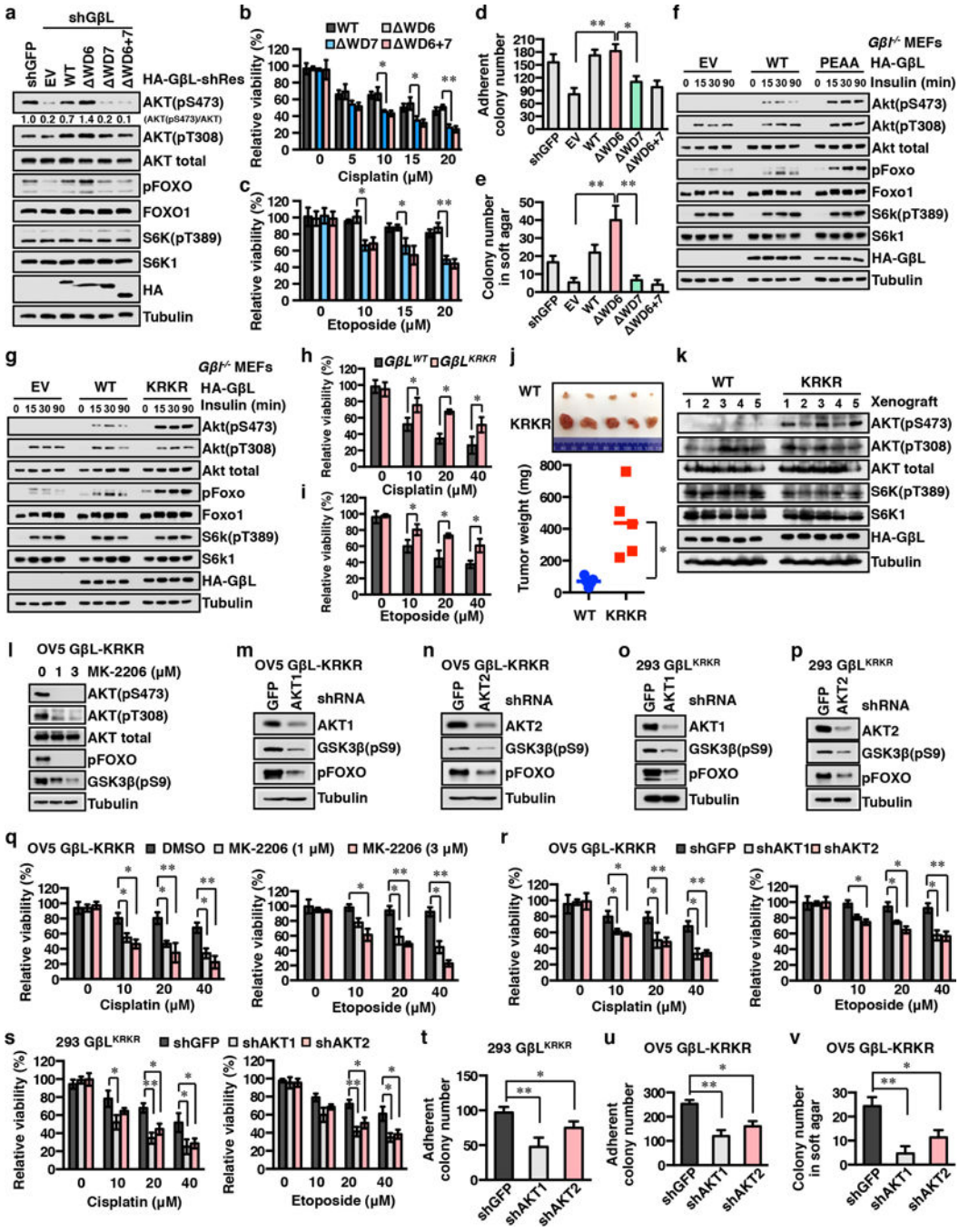

Extended Data Figure 6. Deficiency in GβL ubiquitination favours cell survival through elevating the oncogenic mTORC2/AKT signalling

a, The WD7 motif of GβL is critical for activation of mTORC2 in cells. IB analysis of WCL derived from *GβL*-depleted OVCAR5 cells stably expressing GβL or indicated GβL mutants. **b, c**, The SIN1-specific-interacting GβL WD7 motif is critical to maintain mTORC2/AKT signalling to promote cellular survival. *GβL*-depleted OVCAR5 cells stably

expressing WT or various deletion mutants were exposed to indicated concentrations of cisplatin (**b**) and etoposide (**c**) for 24 h to measure cell viabilities. Data from three independent experiments were presented as mean ± s.d. and analysed by ANOVA (*P < 0.05, **P < 0.01) **d**, **e**, The WD7 motif of GβL is critical for contact-dependent and -independent growth of OVCAR5 cells. Quantification results of colony growth (**d**) or anchorage independent growth (**e**) of *GβL*-depleted OVCAR5 cells stably expressing GβL or indicated GβL mutants. Data were mean ± s.d. from three independent repeats (*P < 0.05, **P < 0.01, ANOVA analysis). **f**, **g**, Deficiency in GβL ubiquitination leads to elevated Akt activation in response to insulin stimulation. $G\beta L^{-/-}$ MEFs stably expressing HA–GβL and the TRAF2 non-interacting HA–GβL(PEAA) mutant (**f**) or the ubiquitinaiton-deficient HA–GβL(KRKR) mutant (**g**) were subjected to serum starvation for 16 h, stimulated with insulin (100 nM) for indicated time points before harvesting for IB analysis of WCL. **h**, **i**, Loss of ubiquitination at endogenous GβL promotes resistance to DNA damage drugs. Wild-type or $G\beta L^{KRKR}$ knock-in HEK293 cells were exposed to indicated concentrations of cisplatin (**h**) and etoposide (**i**) for 24 h to measure cell viabilities (biological triplicates, mean ± s.d., *P < 0.05, two-tailed paired Student's *t*-test). **j**, Representative image of the dissected tumours derived from *GβL*-depleted OVCAR5 cells stably expressing GβL or GβL(KRKR) mutant (upper panel). The weight of individual tumour was shown in the lower panel (n = 5 tumours per group, mean ± s.d., *P < 0.05, two-tailed paired Student's *t*-test). **k**, Loss of GβL ubiquitination leads to elevated AKT activation in the xenograft tumours. IB analysis of WCL derived from dissected xenografts formed by *GβL*-depleted OVCAR5 cells stably expressing GβL or GβL(KRKR) mutant. **l**, The specific AKT kinase inhibitor, MK-2206, inhibits AKT activity in *GβL*-depleted OVCAR5 cells stably expressing GβL(KRKR) cultured in 10% FBS-containing medium. Cells were treated with MK-2206 at indicated concentration for 2 h and lysed for IB analysis. **m**–**p**, Knockdown of endogenous *AKT1* or *AKT2* inhibits the activation of AKT downstream substrates in *GβL*-depleted OVCAR5 cells stably expressing GβL(KRKR) (**m**, **n**) or in $G\beta L^{KRKR}$ knock-in HEK293 cells (**o**, **p**). **q**, **r**, Inhibition of AKT activity by MK-2206 (**q**) or knocking down *AKT1* or *AKT2* (**r**) in *GβL*-depleted OVCAR5 cells stably expressing GβL(KRKR) promotes cell survival. The cells were incubated with indicated concentrations of cisplatin and etoposide for 24 h. The relative cell viabilities were presented as mean ± s.d. from triple repeats (*P < 0.05, **P < 0.01, ANOVA analysis). **s**, Knockdown of *AKT1* or *AKT2* in $G\beta L^{KRKR}$ knock-in HEK293 cells sensitizes these cells to DNA-damaging drugs. The cell viabilities from triple repeats were presented as mean ± s.d. and analysed by ANOVA (*P < 0.05, **P < 0.01). **t**, **u**, AKT activity is critical for contact-dependent and -independent growth of cells expressing the ubiquitination-deficient form of GβL. Quantification of colony growth by $G\beta L^{KRKR}$ knock-in HEK293 cells (**t**) or *GβL*-depleted OVCAR5 cells stably expressing the GβL(KRKR) mutant (**u**), with or without knocking down *AKT1* or *AKT2*. Data were presented as mean ± s.d. and analysed by ANOVA (*P < 0.05, **P < 0.01). **v**, Knockdown of *AKT1* or *AKT2* inhibits anchorage-independent growth of *GβL*-depleted OVCAR5 cells stably expressing GβL(KRKR). Mean ± s.d. (ANOVA analysis, *P < 0.05, **P < 0.01). For uncroppoed gels, see Supplementary Fig. 1. For tumour data, see Source Data.

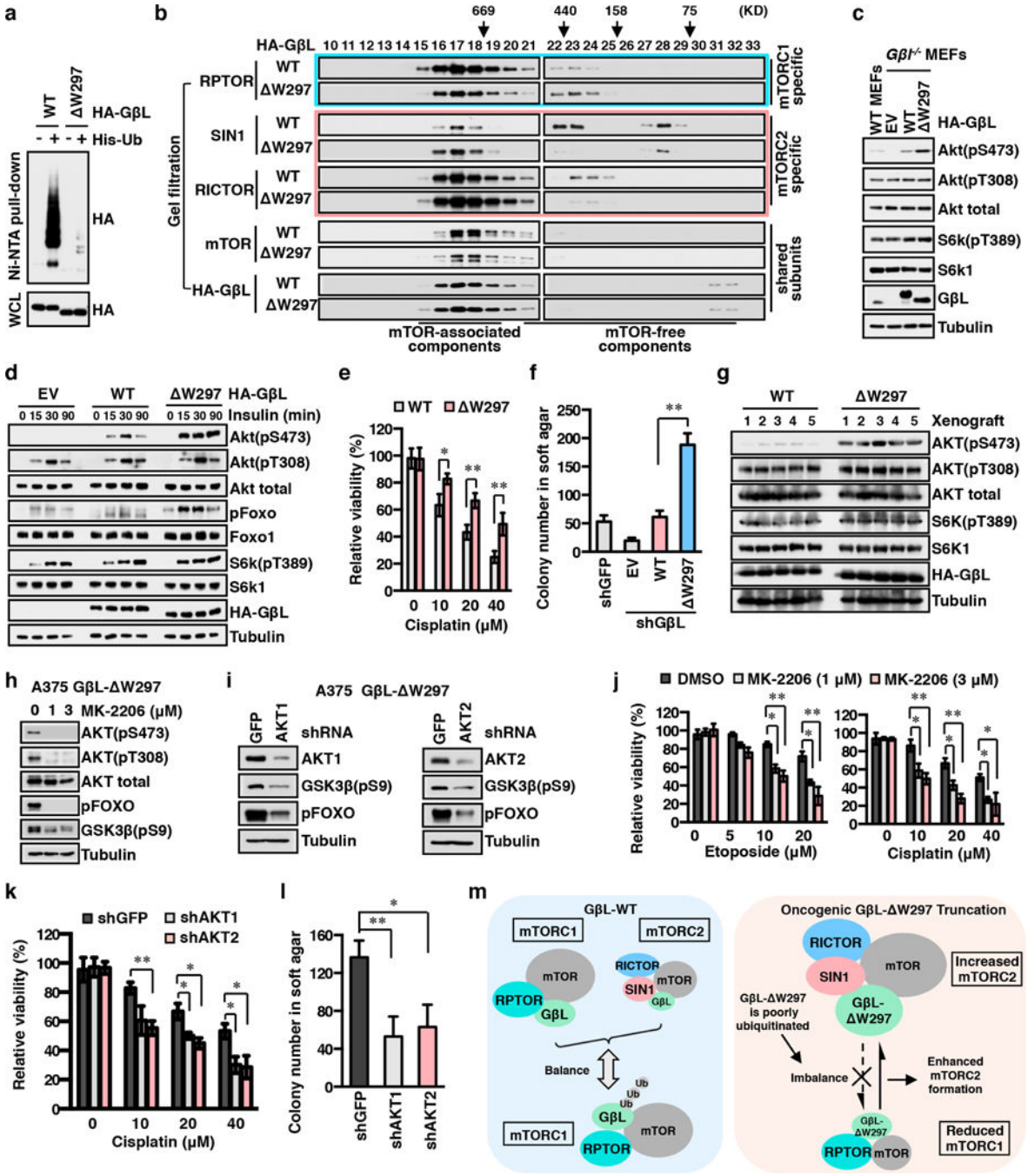

Extended Data Figure 7. Cancer-associated ubiquitination-deficient GβL(ΔW297) truncation mutant promotes tumour growth in part via enhancing mTORC2 formation and activating the oncogenic mTORC2/AKT signaling

a, Compared to wild-type GβL, the cancer-associated GβL(ΔW297) truncation mutant exhibits significantly reduced levels of GβL ubiquitination in cells. Polyubiquitination of GβL in HEK293 cells was examined by transfecting the indicated HA–GβL constructs with His–Ub, followed by IB analysis of WCL and Ni-NTA pull-down products under denaturing conditions. **b**, Reintroducing the GβL(ΔW297) truncation, compared to GβL, into *GβL*-depleted A375 cells leads to relatively increased formation of mTORC2 and reduced

mTORCl. *GβL*-depleted A375 cells stably expressing GβL or GβL(ΔW297) were lysed using CHAPS buffer. WCL was filtrated and run through an FPLC Superdex 200 column to collect fractionated cell eluates for subsequent IB analysis. **c**, Compared to GβL, GβL(ΔW297) is more potent towards activating AKT in cells. IB analysis of WCL derived from $G\beta l^{+/+}$ MEFs or $G\beta l^{-/-}$ MEFs transfected with indicated GβL constructs. **d**, Cancer-associated GβL(ΔW297) truncation enhances mTORC2 activity towards phosphorylating Akt in response to insulin stimulation. $G\beta L^{-/-}$ MEFs stably expressing either HA–GβL or the HA–GβL(ΔW297) mutant were serum starved for 16 h, stimulated with insulin (100 nM) for indicated time points, and lysed for IB analysis of WCL. **e**, Compared to GβL, ectopic expression of the GβL(ΔW297) truncation mutant displays enhanced chemoresistance. *GβL*-depleted A375 cells stably expressing GβL or GβL(ΔW297) were exposed to indicated concentrations of cisplatin for 24 h. The cell viabilities from triple replicates were presented as mean ± s.d. (*$P < 0.05$, **$P < 0.01$, two-tailed paired Student's *t*-test). **f**, Compared to GβL, ectopic expression of the melanoma-associated GβL(ΔW297) truncation is more potent in promoting contact-independent growth of melanoma cells. Representative images of soft agar colony formation by *GβL*-depleted A375 cells stably expressing GβL or GβL(ΔW297) were shown (triplicate independent experiments, mean ± s.d., **$P < 0.01$, two-tailed paired Student's *t*-test). **g**, Loss of GβL ubiquitination leads to elevated AKT activation in the xenograft tumours. IB analysis of lysates derived from dissected xenografts formed by *GβL*-depleted A375 cells stably expressing GβL or the GβL(ΔW297) mutant. **h**, MK-2206 inhibits AKT activity in *GβL*-depleted A375 cells stably expressing GβL(ΔW297). Cells were treated with an AKT inhibitor MK-2206 at 1 or 3 μM (with DMSO as vehicle control) for 2 h and lysed for IB analysis. **i**, Knockdown of *AKT1* or *AKT2* inhibits the activation of AKT downstream substrates in *GβL*-depleted A375 cells stably expressing GβL(ΔW297). **j**, **k**, Inhibition of AKT activity by MK-2206 (**j**) or knocking down of *AKT1* or *AKT2* (**k**) in *GβL*-depleted A375 cells expressing GβL(ΔW297) confers sensitivity to DNA-damaging drugs. Cells were incubated with cisplatin or etoposide for 24 h. The relative cell viabilities from triple repeat were presented as mean ± s.d. and analysed by ANOVA (*$P < 0.05$, **$P < 0.01$). **l**, Knockdown of *AKT1* or *AKT2* inhibits anchorage-independent growth of GβL(ΔW297)-expressing cells A375 cells (three independent experiments, mean ± s.d., ANOVA analysis, *$P < 0.05$, **$P < 0.01$). **m**, A proposed model to describe how the melanoma-associated GβL(ΔW297) truncation mutant disrupts the homeostasis of the two mTOR complexes by impairing polyubiquitination of GβL in cells. Under physiological conditions, the balance of mTORC1 and mTORC2 is tightly controlled by polyubiquitination of GβL on the K305/K313 residues of its WD7 motif. In melanoma cells, the GβL(ΔW297) mutation leads to loss of critical lysine residues for ubiquitination, thus enhancing GβL interaction with SIN1 to promote mTORC2 formation. This subsequently activates the oncogenic AKT signalling to facilitate tumorigenesis. For uncropped gels, see Supplementary Fig. 1.

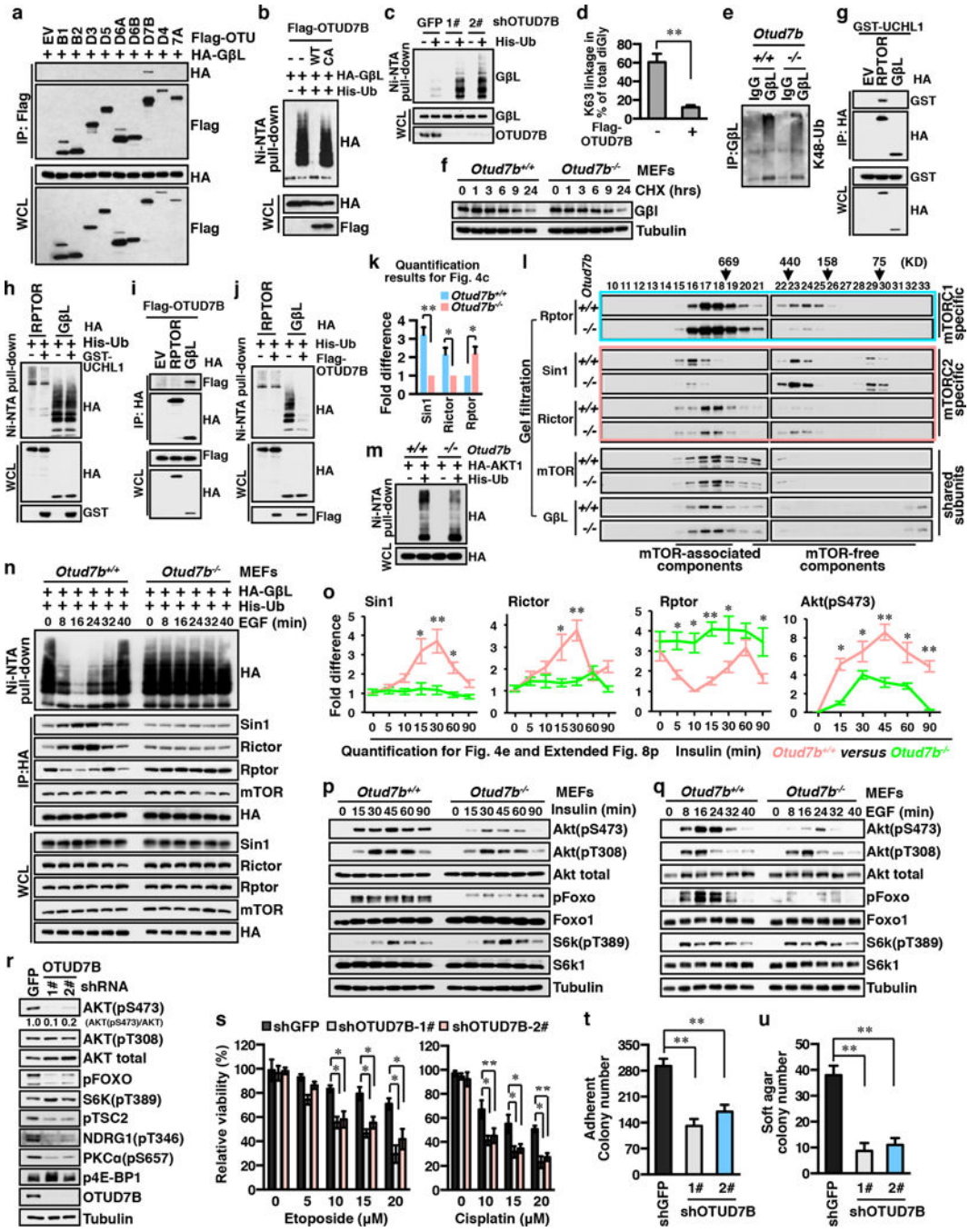

Extended Data Figure 8. OTUD7B deubiquitinates GβL to promote mTORC2 integrity and signalling activity

a, Identification of OTUD7B as a specific GβL-interacting deubiquitinase (DUB). IB analysis of WCL and Flag immunoprecipitate derived from HEK293 cells transfected with HA–GβL and Flag-tagged OTU family members of DUBs. **b**, OTUD7B promotes deubiquitination of GβL in cells in an enzymatic activity-dependent manner. The polyubiquitination status of GβL in HEK293 cells was examined by transfecting HA–GβL and His–Ub with Flag–OTUD7B or activity-deficient OTUD7B(C194A), followed by IB

analysis of WCL and Ni-NTA pull-down products under denaturing conditions. **c**, Knockdown of *OTUD7B* enhances polyubiquitination of endogenous GβL in cells. IB analysis of WCL or Ni-NTA pull-down products under denaturing conditions derived from control or *OTUD7B*-depleted HEK293 cells transfected with His–Ub construct. **d**, K63-linked polyubiquitination of GβL is reduced by ectopic expression of OTUD7B in cells. *OTUD7B*-depleted HEK293 cells were transfected with CMV-GST-GβL and ubiquitin expression constructs, with or without the Flag–OTUD7B vector. Forty-eight hours post-transfection, cells were lysed using Triton buffer for GST pull-down to elute GST–GβL protein for UB-AQUA-MS analysis of ubiquitin chain linkage in total diGly-purified GβL protein (triplicates, mean ± s.d., $^{**}P < 0.01$, two-tailed paired Student's *t*-test). **e**, Depletion of *Otud7b* minimally affects K48-linked polyubiquitination of endogenous GβL. IB analysis of WCL or GβL immunoprecipitate products derived from *Otud7b*$^{+/+}$ and *Otud7b*$^{-/-}$ MEFs transfected with HA–Ub construct. Forty-eight hours post-transfection, the cells were lysed using Triton buffer for GβL immunoprecipitation, with rabbit IgG antibody as negative control. **f**, Depletion of *Otud7b* minimally affects the half-life of endogenous GβL protein in cells. IB analysis of WCL derived from *Otud7b*$^{+/+}$ and *Otud7b*$^{-/-}$ MEFs exposed to cycloheximide (CHX, 100 μg ml^{-1}) at indicated time points before harvesting. **g**, UCH-L1 specifically interacts with RPTOR, but not GβL, in cells. IB analysis of WCL and HA immunoprecipitate derived from HEK293 cells transfected with the GST-UCH-L1 mammalian expression vector, together with HA–RPTOR or HA–GβL plasmids. Cells were lysed using EBC buffer for HA immunoprecipitation procedures. **h**, UCH-L1 deubiquitinates RPTOR, but not GβL, in cells. IB analysis of WCL or Ni-NTA pull-down products under denaturing conditions derived from HEK293 cells transfected with GST-UCH-L1 and His–Ub constructs, together with HA–RPTOR or HA–GβL plasmids as indicated. **i**, OTUD7B specifically interacts with GβL, but not RPTOR, in cells. IB analysis of WCL and HA immunoprecipitate derived from HEK293 cells transfected with Flag–OTUD7B, together with HA–RPTOR or HA–GβL constructs where indicated. The cells were lysed using EBC buffer for immunoprecipitation procedures. **j**, OTUD7B reduces polyubiquitination of GβL, but not RPTOR, in cells. IB analysis of WCL or Ni-NTA pull-down products under denaturing conditions derived from HEK293 cells transfected with Flag–OTUD7B and His–Ub constructs, along with HA–RPTOR or HA–GβL plasmids as indicated. **k**, Quantification results from three independent experiments showing fold differences of endogenous GβL binding to Sin1, Rictor and Rptor in *Otud7b*$^{+/+}$ and *Otud7b*$^{-/-}$ MEFs, as indicated in Fig. 4c. Data are mean ± s.d. The intensity of each blot generated using ImageJ software was analysed by paired Student's *t*-test, $^{*}P < 0.05$, $^{**}P < 0.01$. **l**, Deletion of *Otud7b* reduces formation of endogenous mTORC2, meanwhile increasing the formation of endogenous mTORC1. *Otud7b*$^{+/+}$ and *Otud7b*$^{-/-}$ MEFs in normal culture medium were lysed using CHAPS buffer to preserve mTOR complex integrity. WCL was fractionated through an FPLC Superdex 200 column. Five hundred microlitres of eluate was collected for each fraction for subsequent SDS–PAGE and IB analysis. **m**, Deletion of *Otud7b* does not significantly regulate AKT ubiquitination in cells. IB analysis of WCL or Ni-NTA pull-down products under denaturing conditions derived from *Otud7b*$^{+/+}$ and *Otud7b*$^{-/-}$ MEFs transfected with HA–AKT1 and His–Ub. **n**, Deletion of *Otud7b* leads to constant polyubiquitination of GβL that impairs the dynamic fluctuation in the formation of the two mTOR complexes in response to EGF stimulation. IB analysis of

WCL, HA immunoprecipitate or Ni-NTA pull-down products derived from *Otud7b*$^{+/+}$ and *Otud7b*$^{-/-}$ MEFs transfected with HA–GβL and His–Ub. Thirty-two hours post-transfection, cells were subjected to serum starvation for 16 h, exposed to EGF (100 ng ml^{-1}), and lysed at indicated time points using CHAPS buffer for HA immunoprecipitation or under denaturing buffer for Ni-NTA pull-down procedures. **o**, Quantification results from triple replicates showing fold differences of GβL binding to Sin1, Rictor and Rptor, or the Akt(pS473) levels, in *Otud7b*$^{+/+}$ and *Otud7b*$^{-/-}$ MEFs stably expressing GβL at the indicated time points of insulin stimulation, as indicated in Fig. 4e and Extended Data Fig. 8p. Data are mean ± s.d. The intensity of each blot generated using ImageJ software was analysed by paired Student's *t*-test, **P* < 0.05, ***P* < 0.01. **p**, **q**, Loss of *Otud7b* attenuates mTORC2 kinase activityin response to growth factor stimulation in cells. *Otud7b*$^{+/+}$ and *Otud7b*$^{-/-}$ MEFs were serum starved for 16 h and then treated with insulin (**p**, 100 nM) or EGF (**q**, 100 ng ml^{-1}) for indicated time points, and lysed for IB analysis. **r**, *OTUD7B* knockdown inhibits mTORC2 kinase activity in cells. IB analysis of WCL derived from OVCAR5 cells stably expressing independent OTUD7B-targeting shRNAs (with shGFP as a negative control). For quantification, AKT(pS473) levels were normalized to total AKT and arbitrarily set at 1.0 in the blot of shGFP cells. **s**, *OTUD7B* knockdown sensitizes cells to DNA-damaging drugs. OVCAR5 cells stably expressing independent OTUD7B-targeting lentiviral shRNAs (with shGFP as a negative control) were exposed to etoposide or cisplatin for 24 h to measure cell viabilities. Data from three independent experiments were shown as mean ± s.d. and analysed by ANOVA (**P* < 0.05, ***P* < 0.01). **t**, **u**, Knockdown of *OTUD7B* reduces cell growth and transforming capacity *in vitro*. Quantification results of colony formation (**t**) and soft agar colony growth (**u**) by OVCAR5 cells stably expressing OTUD7B-targeting shRNAs (three independent experiments, mean ± s.d., **P* < 0.05, ***P* < 0.01, ANOVA analysis). For uncropped gels, see Supplementary Fig. 1.

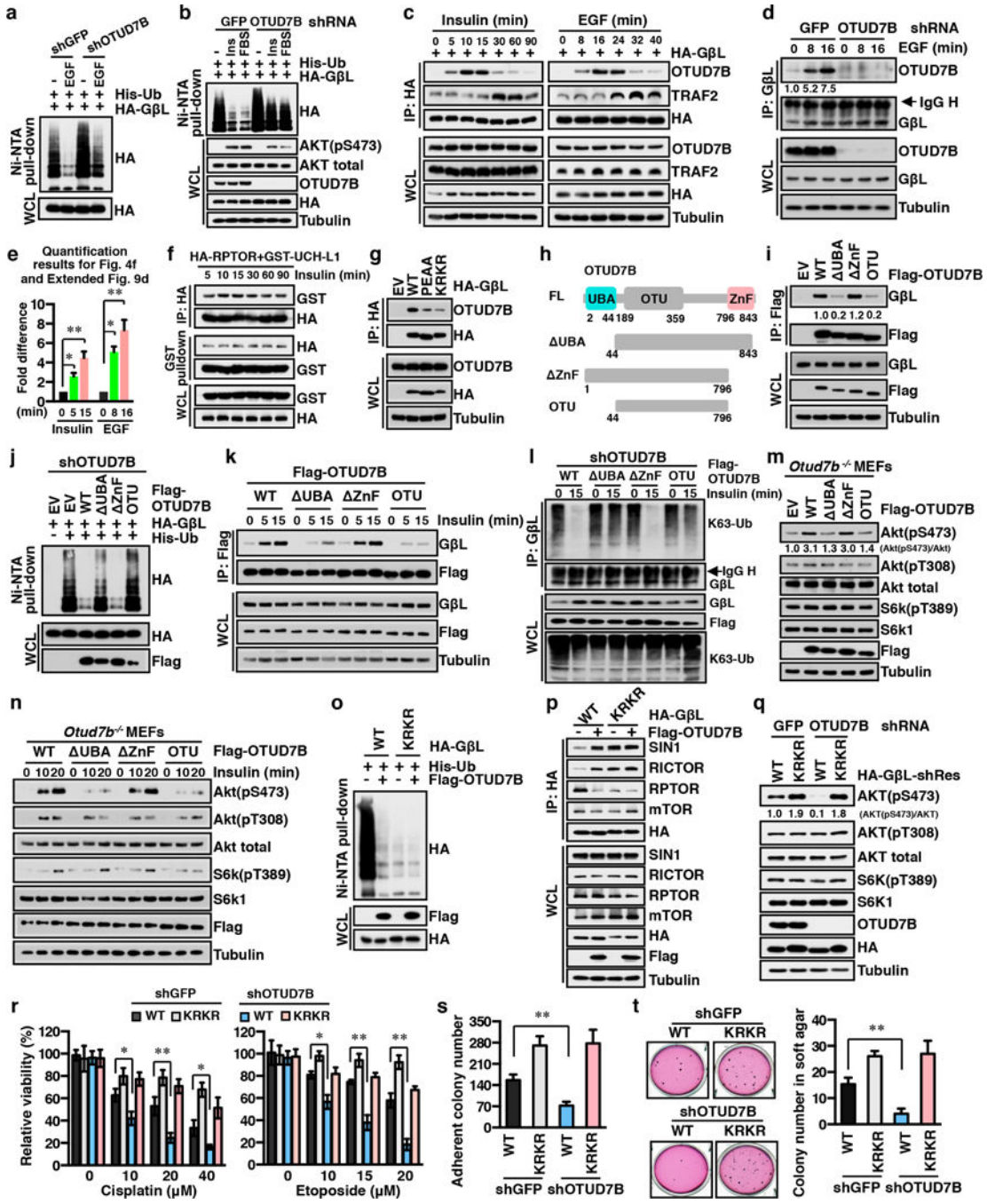

Extended Data Figure 9. Upon physiological stimulation such as growth factor signalling, there is an induced OTUD7B interaction with GβL to enhance mTORC2 activity and oncogenicity primarily through deubiquitinating GβL

a, b, Deletion of *OTUD7B* enhances polyubiquitination of GβL largely in cells stimulated with growth factor signalling. IB analysis of WCL and Ni-NTA pull-down products under denaturing conditions derived from HEK293 cells transfected with His–Ub and HA–GβL constructs. Thirty-two hours post-transfection, cells were subjected to serum starvation for 16 h, stimulated with or without EGF (100 ng ml^{-1}) (**a**) for 16 min, or insulin (100 nM) or 10% FBS-containing medium (**b**) for 30 min, and lysed at indicated time points. **c**, OTUD7B

interaction with GβL in cells is induced by growth factor stimulation. IB analysis of WCL and HA immunoprecipitate derived from HEK293 cells transfected with HA–GβL construct. Thirty-two hours post-transfection, cells were serum starved for 16 h, then exposed to insulin (100 nM) or EGF (100 ng ml^{-1}), and lysed at indicated time points using EBC buffer for the HA immunoprecipitation procedure. **d**, Endogenous OTUD7B interaction with GβL is triggered by EGF stimulation. IB analysis of GβL immunoprecipitate or WCL derived from HEK293 cells with or without knockdown of endogenous OTUD7B. Cells were serum starved for 16 h, then stimulated with EGF (100 ng ml^{-1}), and lysed at indicated time points using EBC buffer for immunoprecipitation and IB analysis. See **e** for quantification results, with levels arbitrarily set to 1.0 at the 0 min time point. **e**, Quantification results showing fold differences of endogenous GβL binding to OTUD7B in cells at the indicated time points of growth factor stimulation, as indicated in **d** and Fig. 4f. Data are mean ± s.d. The intensity of each blot from three independent experiments was measured using ImageJ software and analysed by ANOVA, $*P < 0.05$, $**P < 0.01$. **f**, Unlike OTUD7B, UCH-L1 interaction with RPTOR is not regulated by growth stimulation. IB analysis of WCL, GST pull-down products and HA immunoprecipitate derived from HEK293 cells transfected with HA–RPTOR and the GST-UCH-L1 mammalian expression constructs. Thirty-two hours post-transfection, cells were serum starved for 16 h, stimulated with insulin (100 nM) and lysed using EBC buffer at indicated time points for the HA immunoprecipitation procedure. For quantification analysis of endogenous GβL binding to other components, levels were arbitrarily set to 1.0 at the 0 min time point. **g**, OTUD7B displays a reduced binding affinity to ubiquitination-deficient GβL. IB analysis of WCL and HA immunoprecipitate derived from HEK293 cells transfected with wild-type GβL, GβL(KRKR), or TRAF2-non-interacting GβL(PEAA) constructs. **h**, A schematic illustration showing different domains of the human OTUD7B protein, as well as various OTUD7B mutants used in this study. **i**, Deletion of the OTUD7B UBA domain impairs OTUD7B interaction with endogenous GβL. IB analysis of WCL and Flag immunoprecipitate derived from HEK293 cells transfected with OTUD7B or indicated OTUD7B mutant constructs. For quantification results of OTUD7B binding to endogenous GβL levels, levels were arbitrarily set to 1.0 in blot of OTUD7B-expressing cells. **j**, The UBA domain of OTUD7B is critical for its deubiquitinase activity towards GβL in cells. IB analysis of WCL and Ni-NTA pull-down products under denaturing conditions derived from HEK293 cells transfected with His–Ub and HA–GβL constructs, together with OTUD7B or indicated OTUD7B mutant constructs. **k**, Deletion of the OTUD7B UBA domain impairs growth-factor-induced OTUD7B interaction with GβL. IB analysis of WCL and Flag immunoprecipitate derived from HEK293 cells transfected with OTUD7B or indicated OTUD7B mutant constructs. Thirty-two hours post-transfection, cells were serum starved for 16 h, stimulated with insulin (100 nM) and lysed using EBC buffer at indicated time points for the immunoprecipitation procedure. **l**, Deletion of the OTUD7B UBA domain attenuates growth-factor-induced OTUD7B-mediated de-ubiquitination of GβL. IB analysis of WCL and GβL immunoprecipitate products derived from *OTUD7B*-depleted HEK293 cells stably expressing OTUD7B or indicated OTUD7B mutants. Cells were transfected with His–Ub constructs for 32 h, subjected to serum starvation for 16 h, and then stimulated with or without insulin (100 nM) and lysed using EBC buffer at indicated time points for subsequent IP procedure. **m**, **n**, Deletion of the OTUD7B UBA domain attenuates activation of the downstream mTORC2/AKT oncogenic

signalling. IB analysis of WCL derived from *Otud7b*$^{-/-}$ MEFs stably expressing OTUD7B or indicated OTUD7B mutants. The cells were either cultured in 10% FBS-containing culture medium (**m**), or subjected to serum starvation for 16 h, and then stimulated with or without insulin (**n**, 100 nM) and lysed using EBC buffer at indicated time points for IB analysis. For quantification, Akt(pS473) levels were normalized to total Akt and arbitrarily set to 1.0 in the first lane. **o**, OTUD7B promotes deubiquitination of wild-type GβL, but not the GβL(KRKR) mutant, in cells. IB analysis of WCL and Ni-NTA pull-down products under denaturing conditions derived from HEK293 cells transfected with His–Ub and HA–GβL or the ubiquitination-deficient HA–GβL(KRKR) mutant constructs, along with or without Flag–OTUD7B as indicated. **p**, OTUD7B promotes the integration of GβL, but not GβL(KRKR), into mTORC2 in cells. IB analysis of WCL and HA immunoprecipitate derived from HEK293 cells transfected with HA–GβL or the HA–GβL(KRKR) mutant, together with or without Flag–OTUD7B as indicated. Forty-eight hours post-transfection, cells were lysed using CHAPS buffer for the HA immunoprecipitation procedure to maintain mTOR complex integrity. **q**, OTUD7B regulates AKT activity primarily through modulating the ubiquitination status of GβL. IB analysis of WCL derived from OTUD7B-depleted or control OVCAR5 cells stably expressing GβL or GβL(KRKR). For quantification of AKT(pS473), levels were normalized to total AKT and arbitrarily set to 1.0 in the first lane. **r**, OTUD7B governs chemoresistance primarily through modulating the ubiquitination status of GβL. shGFP-infected control or *OTUD7B*-depleted OVCAR5 cells stably expressing GβL or the GβL(KRKR) mutant were exposed to cisplatin or etoposide for 24 h. Data from three independent experiments were presented as mean ± s.d. and analysed by ANOVA (*P < 0.05, **P < 0.01). **s**, **t**, OTUD7B enhances colony growth and anchorage-independent growth of tumour cells primarily through deubiquitinating GβL in cells. Quantitative data of colony growth in plates (**s**) and in soft agar (**t**) by control or *OTUD7B*-depleted OVCAR5 cells stably expressing GβL or the GβL(KRKR) mutant. Representative images of soft agar colonies are shown in **t**. The result from triple experiments were presented as mean ± s.d. and analysed by ANOVA (**P < 0.01). For uncropped gels, see Supplementary Fig. 1.

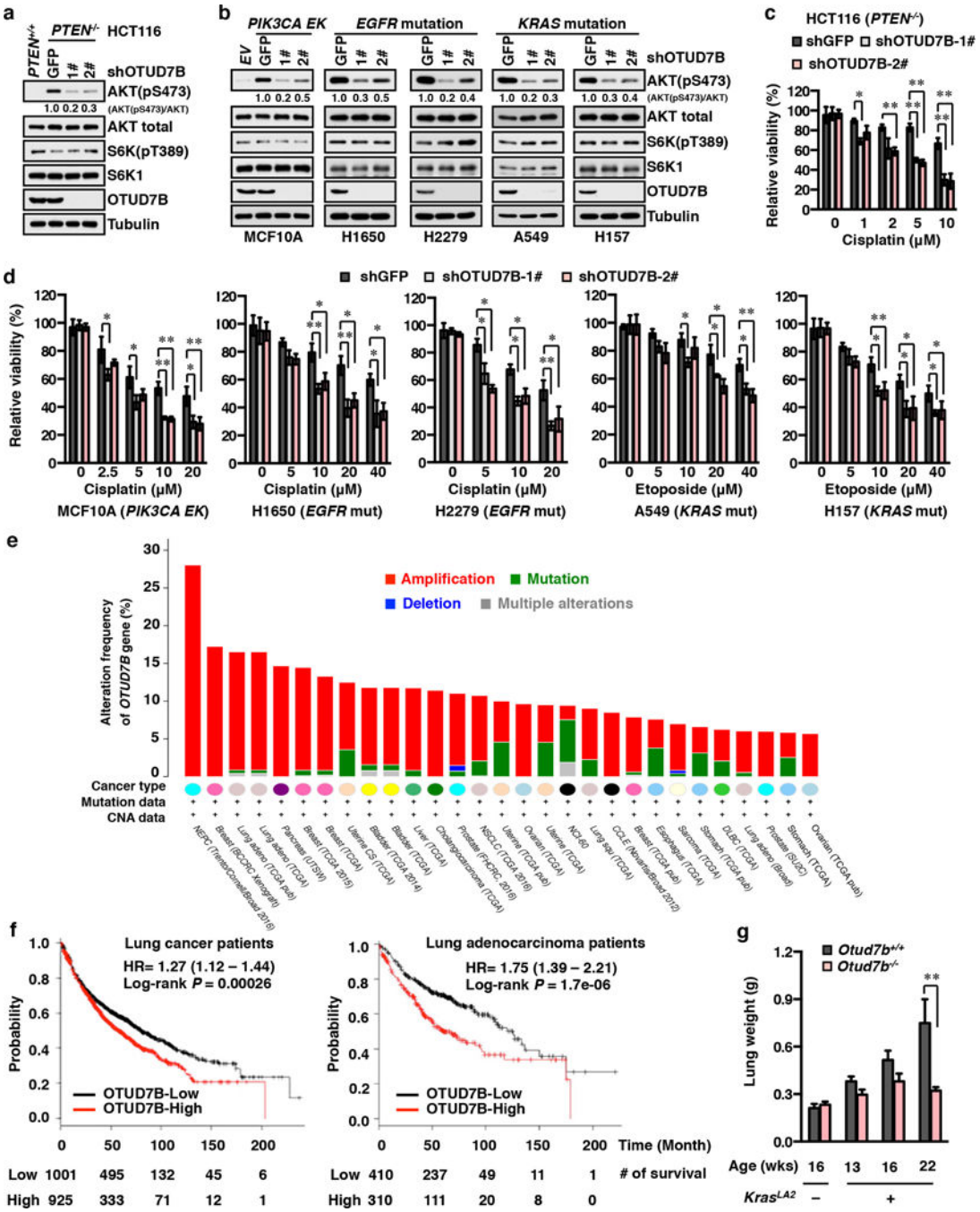

Extended Data Figure 10. Downstream of various oncogenic mutations, OTUD7B-mediated activation of mTORC2/AKT signalling plays a physiological role in promoting cancer development

a, b, Knockdown of endogenous *OTUD7B* suppresses AKT(pS473) levels in several cancer cell lines in which mTORC2/AKT oncogenic signalling was activated by various upstream oncogenic events. IB analysis of WCL derived from HCT116 (**a**, *PTEN* deletion), MCF10A (**b**, *PIK3CA EK* mutation), H1650 and H2279 (**b**, *EGFR* mutation), and A549 and H157 (**b**, *KRAS* mutation) cell lines stably expressing independent OTUD7B-targeting lentiviral shRNAs (with shGFP as a negative control). For quantification results of AKT(pS473)

levels, levels were normalized to total AKT and arbitrarily set to 1.0 in the blot of shGFP-expressing cells. **c**, **d**, Knockdown of endogenous *OTUD7B* sensitizes cancer cells to chemotherapeutic drugs. HCT116 (**c**, *PTEN* deletion), MCF10A (**d**, *PIK3CA EK* mutation), H1650 and H2279 (**d**, *EGFR* mutation), and A549 and H157 (**d**, *KRAS* mutation) cells stably expressing independent OTUD7B-targeting lentiviral shRNAs were exposed to indicated concentrations of cisplatin or etoposide for 24 h. Cell viability data from triple replicates are presented as mean ± s.d. and were analysed by ANOVA (*$P < 0.05$, **$P < 0.01$). **e**, TCGA DNA sequencing results showing that the *OTUD7B* gene is amplified at high frequencies in a variety of human cancers, such as breast, lung and pancreatic cancers. **f**, Kaplan–Meier analysis showing a tight correlation between OTUD7B expression levels and patient survival. Data were from lung cancer patients with low (n = 1,001) and high (n = 925) OTUD7B expression (left panel), and lung adenocarcinoma patients with low (n = 410) and high (n = 310) OTUD7B expression (right panel). Patient number at risk at different times of analyses is indicated at the bottom of the plots. The plots were generated using the KmPlot tool (http://www.kmplot.com/lung). Affymetrix ID 220031_at was used for analyses. **g**, Lung weight of $Otud7b^{+/+}$ and $Otud7b^{-/-}$ mice, with (+) or without (−)$Kras^{LA2}$ transgene expression, at the indicated ages. Data were presented as mean mean ± s.e.m. (16 weeks: $Otud7b^{+/+}$ mice, n = 6; $Otud7b^{-/-}$ mice, n = 3; 13 weeks: $Otud7b^{+/+}Kras^{LA2}$ mice, n = 5; $Otud7b^{-/-}Kras^{LA2}$ mice, n = 5; 16 weeks: $Otud7b^{+/+}Kras^{LA2}$ mice, n = 8; $Otud7b^{-/-}Kras^{LA2}$ mice, n = 7; 23 weeks: $Otud7b^{+/+}Kras^{LA2}$ mice, n = 7; $Otud7b^{-/-}Kras^{LA2}$ mice, n = 11; **$P < 0.01$, two-tailed unpaired Student's t-test). For uncropped gels, see Supplementary Fig. 1. For tumour data, see Source Data for **g**.

Supplementary Material

Refer to Web version on PubMed Central for supplementary material.

Acknowledgments

We thank T Jacks and the NCI Mouse Repository for providing the $Kras^{LA2}$ mice. We thank P P Pandolfi (Harvard), B. D. Manning (Harvard), and A. Toker (Harvard) for their insightful suggestions and critiques during the preparation of this manuscript. We also thank all Wei laboratory members for critical reading of the manuscript. W.W. is a LLS research scholar. PL. is supported by ROOCA181342. W.G. is supported by 1K99CA207867.

A.O. was supported by an Edward R. and Anne G. Lefler Center postdoctoral fellowship. This work was supported by NIH grants (W.W., R01CA177910 and R01GM094777; S.-C.S., R37AI064639 and R01GM084459; J.W.H., AG011085 and GM095567) and the National Natural Science Foundation of China (B.W., 81472294, L.Z., 81521064).

References

1. Zoncu R, Efeyan A, Sabatini D. M mTOR: from growth signal integration to cancer, diabetes and ageing. Nat Rev Mol Cell Biol. 2011; 12:21–35. [PubMed: 21157483]
2. Aylett CH, et al. Architecture of human mTOR complex 1. Science. 2016; 351:48–52. [PubMed: 26678875]
3. Sancak Y, et al. The Rag GTPases bind raptor and mediate amino acid signaling to mTORC1. Science. 2008; 320:1496–1501. [PubMed: 18497260]
4. Zoncu R, et al. mTORC1 senses lysosomal amino acids through an inside-out mechanism that requires the vacuolar H^+-ATPase. Science. 2011; 334:678–683. [PubMed: 22053050]

5. Bar-Peled L, Schweitzer LD, Zoncu R, Sabatini DM. Ragulator is a GEF for the rag GTPases that signal amino acid levels to mTORC1. Cell. 2012; 150:1196–1208. [PubMed: 22980980]
6. Bar-Peled L, et al. A tumor suppressor complex with GAP activity for the Rag GTPases that signal amino acid sufficiency to mTORC1. Science. 2013; 340:1100–1106. [PubMed: 23723238]
7. Inoki K, Li Y, Xu T, Guan KL. Rheb GTPase is a direct target of TSC2 GAP activity and regulates mTOR signaling. Genes Dev. 2003; 17:1829–1834. [PubMed: 12869586]
8. Guertin DA, Sabatini DM. Defining the role of mTOR in cancer. Cancer Cell. 2007; 12:9–22. [PubMed: 17613433]
9. Liu P, et al. Sin1 phosphorylation impairs mTORC2 complex integrity and inhibits downstream Akt signalling to suppress tumorigenesis. Nat Cell Biol. 2013; 15:1340–1350. [PubMed: 24161930]
10. Liu P, et al. PtdIns(3,4,5)P3-dependent activation of the mTORC2 kinase complex. Cancer Discov. 2015; 5:1194–1209. [PubMed: 26293922]
11. Kim DH, et al. mTOR interacts with raptor to form a nutrient-sensitive complex that signals to the cell growth machinery. Cell. 2002; 110:163–175. [PubMed: 12150925]
12. Yang Q, Inoki K, Ikenoue T, Guan KL. Identification of Sin1 as an essential TORC2 component required for complex formation and kinase activity. Genes Dev. 2006; 20:2820–2832. [PubMed: 17043309]
13. Jacinto E, et al. SIN1/MIP1 maintains rictor-mTOR complex integrity and regulates Akt phosphorylation and substrate specificity. Cell. 2006; 127:125–137. [PubMed: 16962653]
14. Frias MA, et al. mSin1 is necessary for Akt/PKB phosphorylation, and its isoforms define three distinct mTORC2s. Curr Biol. 2006; 16:1865–1870. [PubMed: 16919458]
15. Guertin DA, et al. Ablation in mice of the mTORC components raptor, rictor, or mLST8 reveals that mTORC2 is required for signaling to Akt-FOXO and PKCα, but not S6K1. Dev Cell. 2006; 11:859–871. [PubMed: 17141160]
16. Komander D, Rape M. The ubiquitin code. Annu Rev Biochem. 2012; 81:203–229. [PubMed: 22524316]
17. Ikeda F, Crosetto N, Dikic I. What determines the specificity and outcomes of ubiquitin signaling? Cell. 2010; 143:677–681. [PubMed: 21111228]
18. Linares JF, et al. K63 polyubiquitination and activation of mTOR by the p62-TRAF6 complex in nutrient-activated cells. Mol Cell. 2013; 51:283–296. [PubMed: 23911927]
19. Jin G, et al. Skp2-mediated RagA ubiquitination elicits a negative feedback to prevent amino-acid-dependent mTORC1 hyperactivation by recruiting GATOR1. Mol Cell. 2015; 58:989–1000. [PubMed: 26051179]
20. Deng L, et al. The ubiquitination of rag A GTPase by RNF152 negatively regulates mTORC1 activation. Mol Cell. 2015; 58:804–818. [PubMed: 25936802]
21. Inoki K, Li Y, Zhu T, Wu J, Guan KL. TSC2 is phosphorylated and inhibited by Akt and suppresses mTOR signalling. Nat Cell Biol. 2002; 4:648–657. [PubMed: 12172553]
22. Guertin DA, et al. mTOR complex 2 is required for the development of prostate cancer induced by Pten loss in mice. Cancer Cell. 2009; 15:148–159. [PubMed: 19185849]
23. Mevissen TE, et al. OTU deubiquitinases reveal mechanisms of linkage specificity and enable ubiquitin chain restriction analysis. Cell. 2013; 154:169–184. [PubMed: 23827681]
24. Hussain S, et al. Ubiquitin hydrolase UCH-L1 destabilizes mTOR complex 1 by antagonizing DDB1-CUL4-mediated ubiquitination of raptor. Mol Cell Biol. 2013; 33:1188–1197. [PubMed: 23297343]
25. Mevissen TE, et al. Molecular basis of Lys11-polyubiquitin specificity in the deubiquitinase Cezanne. Nature. 2016; 538:402–405. [PubMed: 27732584]
26. Bremm A, Freund SM, Komander D. Lys11-linked ubiquitin chains adopt compact conformations and are preferentially hydrolyzed by the deubiquitinase Cezanne. Nat Struct Mol Biol. 2010; 17:939–947. [PubMed: 20622874]
27. Gupta S, et al. Binding of ras to phosphoinositide 3-kinase p110alpha is required for ras-driven tumorigenesis in mice. Cell. 2007; 129:957–968. [PubMed: 17540175]
28. Castellano E, et al. Requirement for interaction of PI3-kinase p110α with RAS in lung tumor maintenance. Cancer Cell. 2013; 24:617–630. [PubMed: 24229709]

29. Hu H, et al. OTUD7B controls non-canonical NF-κB activation through deubiquitination of TRAF3. Nature. 2013; 494:371–374. [PubMed: 23334419]
30. Pareja F, et al. Deubiquitination of EGFR by Cezanne-1 contributes to cancer progression. Oncogene. 2012; 31:4599–4608. [PubMed: 22179831]
31. Yuan L, et al. Deubiquitylase OTUD3 regulates PTEN stability and suppresses tumorigenesis. Nat Cell Biol. 2015; 17:1169–1181. [PubMed: 26280536]
32. Bremm A, Moniz S, Mader J, Rocha S, Komander D. Cezanne (OTUD7B) regulates HIF-1α homeostasis in a proteasome-independent manner. EMBO Rep. 2014; 15:1268–1277. [PubMed: 25355043]
33. Wei W, Jobling WA, Chen W, Hahn WC, Sedivy JM. Abolition of cyclin-dependent kinase inhibitor p16Ink4a and p21Cip1/Waf1 functions permits Ras-induced anchorage-independent growth in telomerase-immortalized human fibroblasts. Mol Cell Biol. 2003; 23:2859–2870. [PubMed: 12665584]
34. Gan W, et al. SPOP promotes ubiquitination and degradation of the ERG oncoprotein to suppress prostate cancer progression. Mol Cell. 2015; 59:917–930. [PubMed: 26344095]
35. Ordureau A, et al. Defining roles of PARKIN and ubiquitin phosphorylation by PINK1 in mitochondrial quality control using a ubiquitin replacement strategy. Proc Natl Acad Sci USA. 2015; 112:6637–6642. [PubMed: 25969509]
36. Ordureau A, et al. Quantitative proteomics reveal a feedforward mechanism for mitochondrial PARKIN translocation and ubiquitin chain synthesis. Mol Cell. 2014; 56:360–375. [PubMed: 25284222]
37. Phu L, et al. Improved quantitative mass spectrometry methods for characterizing complex ubiquitin signals. Mol Cell Proteomics. 2011; 10003756:M110.
38. MacLean B, et al. Skyline: an open source document editor for creating and analyzing targeted proteomics experiments. Bioinformatics. 2010; 26:966–968. [PubMed: 20147306]
39. Huttlin EL, et al. A tissue-specific atlas of mouse protein phosphorylation and expression. Cell. 2010; 143:1174–1189. [PubMed: 21183079]
40. Beausoleil SA, Villén J, Gerber SA, Rush J, Gygi S. R A probability-based approach for high-throughput protein phosphorylation analysis and site localization. Nat Biotechnol. 2006; 24:1285–1292. [PubMed: 16964243]
41. Kim W, et al. Systematic and quantitative assessment of the ubiquitin-modified proteome. Mol Cell. 2011; 44:325–340. [PubMed: 21906983]
42. Ran FA, et al. Genome engineering using the CRISRR-Cas9 system. Nat Protocols. 2013; 8:2281–2308. [PubMed: 24157548]
43. Sarbassov DD, et al. Rictor, a novel binding partner of mTOR, defines a rapamycin-insensitive and raptor-independent pathway that regulates the cytoskeleton. Curr Biol. 2004; 14:1296–1302. [PubMed: 15268862]
44. Johnson L, et al. Somatic activation of the *K-ras* oncogene causes early onset lung cancer in mice. Nature. 2001; 410:1111–1116. [PubMed: 11323676]
45. Győrffy B, Surowiak R, Budczies J, Lánczky A. Online survival analysis software to assess the prognostic value of biomarkers using transcriptomic data in non-small-cell lung cancer. PLoS One. 2013; 8:e82241. [PubMed: 24367507]

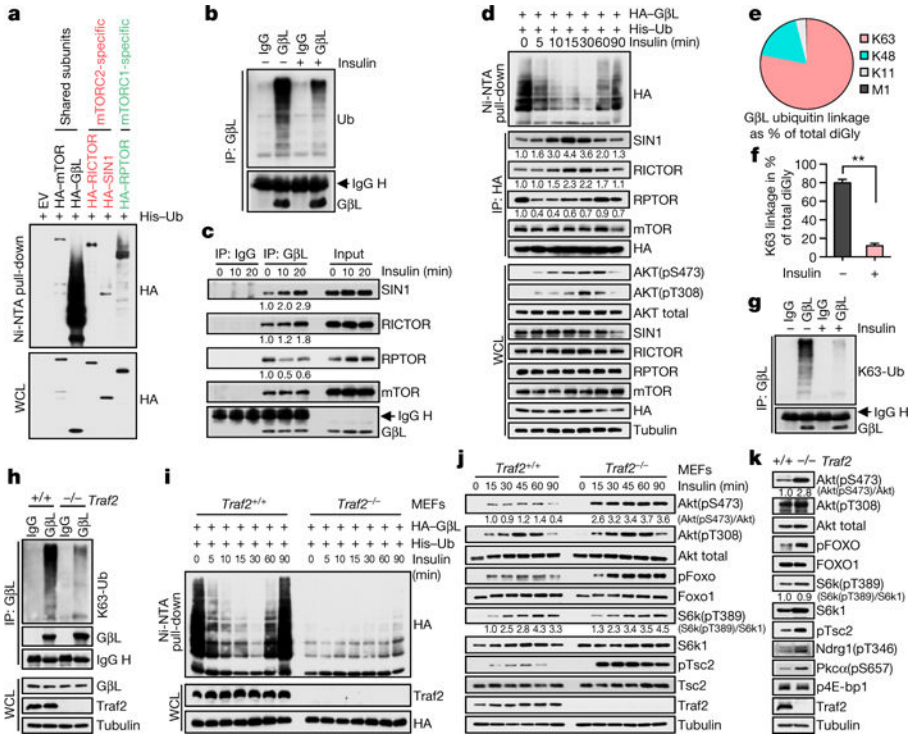

Figure 1. TRAF2 promotes K63-linked polyubiquitination of GβL

a, GβL, and to a lesser extent, RPTOR, are polyubiquitinated in cells. Immunoblot of whole-cell lysates (WCL) and nickel-nitrilotriacetic acid (Ni-NTA) pull-downs from HEK293 cells transfected with His–ubiquitin (His–Ub) and haemagglutinin (HA)-tagged constructs. **b**, Reduced GβL polyubiquitination upon growth factor stimulation. HEK293 cells transfected with ubiquitin constructs were lysed using Triton buffer for anti-GβL immunoprecipitation (IP) and immunoblot. **c**, Dynamic assembly of mTOR complexes upon growth factor stimulation. Serumstarved HEK293 cells were stimulated with insulin and lysed using CHAPS buffer for anti-GβL immunoprecipitation and immunoblot. **d**, Immunoblot of ubiquitinated species, HA immunoprecipitate and WCL derived from insulin-stimulated HEK293 cells transfected with indicated constructs. **e**, **f**, Ubiquitin absolute quantification mass spectrometry (UB-AQUA-MS) analysis of ubiquitin chain linkages of ectopically expressed GβL in serum-starved HEK293 cells (**e**) or cells stimulated by insulin for 15 min (**f**). diGly, Gly-Gly-containing peptides. Data are representative of triplicates, mean ± s.d., ** $P < 0.01$, Student's *t*-test. **g**, **h**, Insulin stimulation or *Traf2* deletion reduces K63 polyubiquitination of GβL. Immunoblot of anti-GβL immunoprecipitate or WCL from insulin-stimulated HEK293 cells (**g**) or *Traf2*$^{+/+}$ and *Traf2*$^{-/-}$ MEFs (**h**). **i**–**k**, Immunoblot of Ni-NTA pull-downs or WCL from *Traf2*$^{+/+}$ and *Traf2*$^{-/-}$ MEFs with (**i**, **j**) or without (**k**) insulin stimulation. For uncropped gels, see Supplementary Fig. 1.

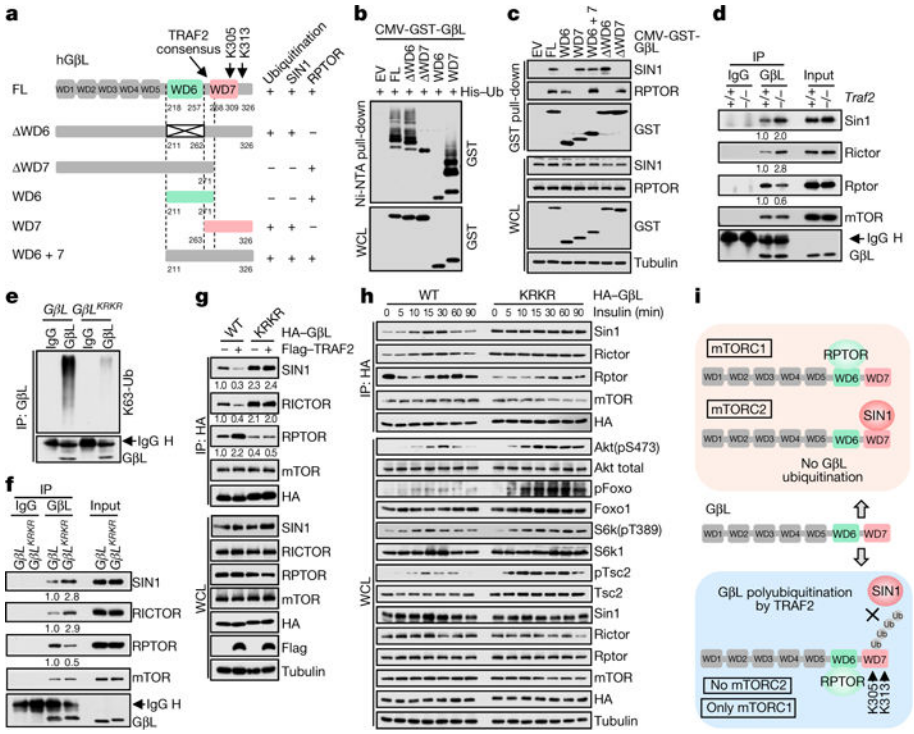

Figure 2. Ubiquitination of GβL on K305 and K313 by TRAF2 governs the homeostasis of mTORC2 kinase

a, WD7 is the major GβL domain undergoing ubiquitination and mediating SIN1 interaction. **b, c**, Immunoblot of Ni-NTA (**b**) or GST pull-downs (**c**) from HEK293 cells transfected with GST-GPL plasmids. CMV, cytomegalovirus promoter. EV, empty vector. FL, full length. **d-f**, Immunoblot of anti-GβL immunoprecipitate from *Traf2*$^{+/+}$ and *Traf2*$^{-/-}$ MEFs (**d**), or wild-type (WT) versus CRISPR-generated *GβL*^{KRKR} knock-in cells (**e, f**). **g**, Immunoblot of HA immunoprecipitate and WCL from HEK293 cells transfected with indicated constructs. **h**, Serum-starved *Gβl*$^{-/-}$ MEFs stably expressing GβL or GβL(KRKR) were exposed to insulin and lysed for immunoblot of WCL and HA immunoprecipitate. i, A model describing GβL polyubiquitination-mediated regulation of dynamic assembly of mTOR complexes. For uncropped gels, see Supplementary Fig. 1.

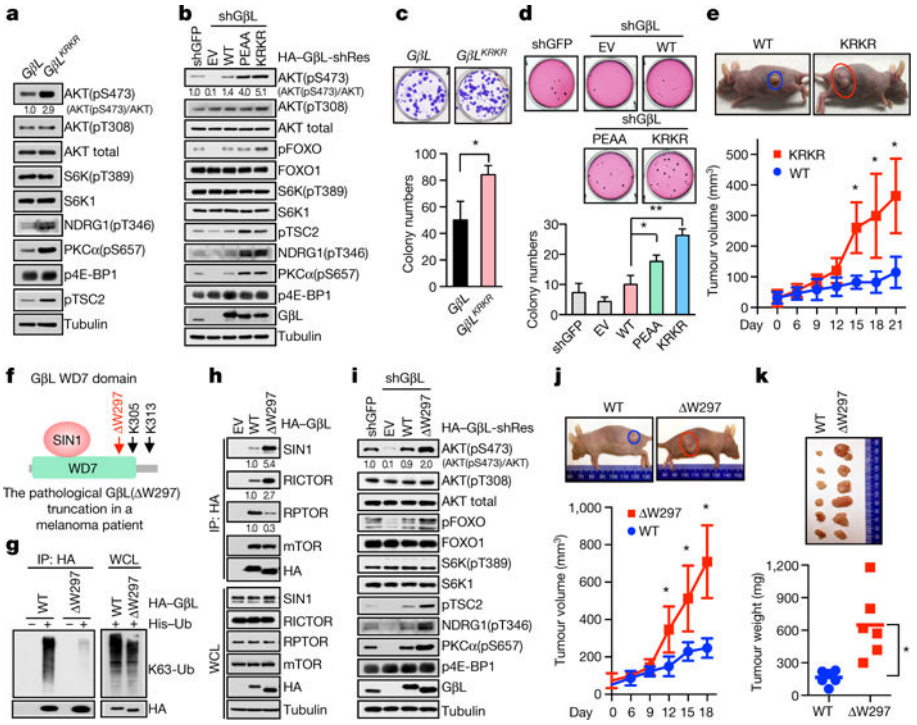

Figure 3. Deficiency in GβL ubiquitination elevates mTORC2 activity to confer oncogenicity

a, b, Loss of GβL ubiquitination enhances AKT activation. Immunoblot of WCL from wild-type or *GβL*^{KRKR} knock-in HEK293 cells (a), or *GβL*-depleted OVCAR5 cells stably expressing GβL or mutants (**b**). shGβL, GβL short hairpin RNA; shRes, mutants resistant to shRNA interference. **c-e**, Deficiency in GβL ubiquitination elevates oncogenicity. c, Colony formation by wild-type or *GβL*^{KRKR} knock-in cells. **d, e**, Soft agar assay (**d**) and growth curve of subcutaneous xenografts (**e**, $n = 6$ nude mice per group) by *GβL*-depleted OVCAR5 cells stably expressing GβL or mutants. Data are representative of triplicates, mean ± s.d., $*P < 0.05$, $**P < 0.01$, Student's *t*-test (**c, e**) or ANOVA analysis (**d**). **f-i**, GβL-ΔW297 truncation (**f**) leads to reduced K63-linked ubiquitination (**g**), enhanced mTORC2 formation (**h**) and activity (**i**) in cells. Immunoblot of HA immunoprecipitate and WCL from cells transfected with indicated constructs (**g, h**), or *GβL*-depleted A375 cells stably expressing GβL or GβL(AW297) (**i**). **j, k**, Growth curve (**j**) and weight (**k**) of subcutaneous tumours formed by *GβL*-depleted A375 cells expressing GβL or GβL(ΔW297) (mean ± s.d., $n = 7$ nude mice (**j**) or 6 tumours (**k**) per group; $*P < 0.05$, $**P < 0.01$, Student's *t*-test). For uncropped gels, see Supplementary Fig. 1. For tumour data, see Source Data for **e, j, k**.

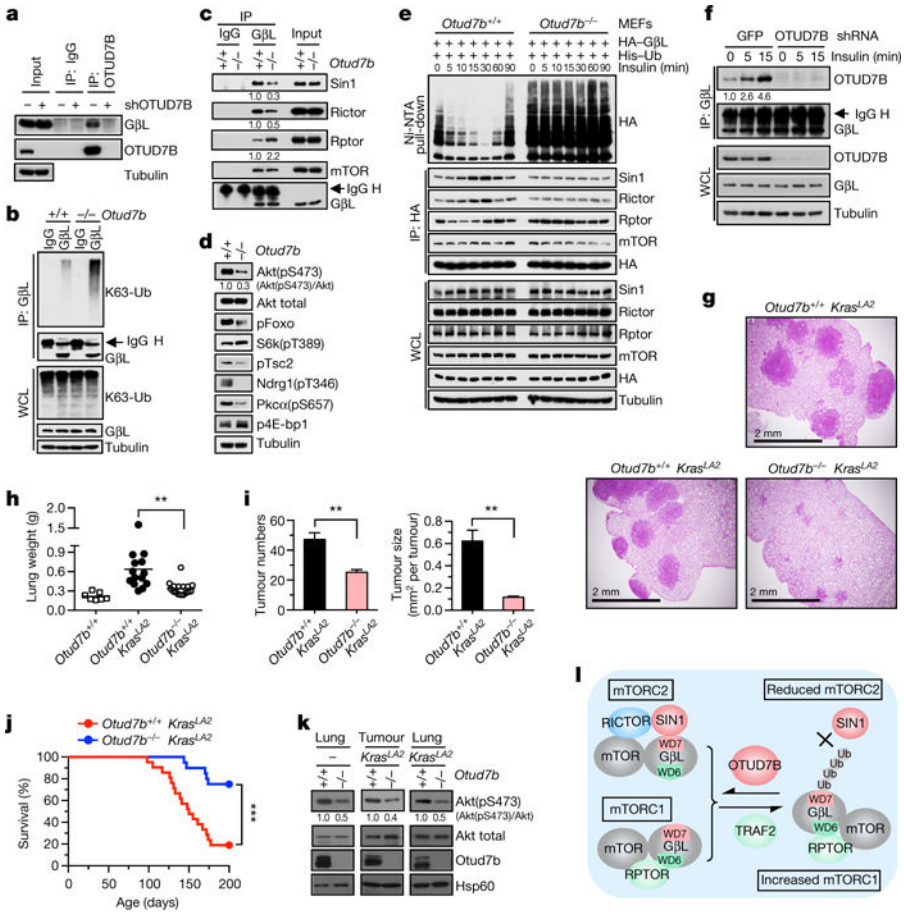

Figure 4. Growth factor signalling triggers TUD7B-mediated GβL deubiquitination to promote mTORC2 integrity, favouring tumorigenesis

a, OTUD7B interacts with GβL at endogenous levels. Immunoblot of WCL and anti-OTUD7B immunoprecipitate from HEK293 cells. **b**–**e**, Depletion of *Otud7b* elevates GβL K63 polyubiquitination, reduces mTORC2 complex formation and activity. Immunoblot analysis of anti-GβL immunoprecipitate, HA immunoprecipitate, Ni-NTA pull-downs or WCL from *Otud7b*$^{+/+}$ and *Otud7b*$^{-/-}$ MEFs in serum-containing medium (**b**–**d**) or upon insulin stimulation (**e**). **f**, OTUD7B interaction with GβL is induced by growth factor stimulation. Immunoblot analysis of anti-GβL immunoprecipitate or WCL from HEK293 cells. **g**–**i**, *Otud7b* deficiency in mice inhibits *Kras*-driven lung tumorigenesis. Histology of lung tissue (**g**; $n = 10$ mice at 16 weeks), lung weight (**h**; *Otud7b*$^{+/+}$, $n = 7$ or *Otud7b*$^{+/+}$*KrasLA2*, $n = 14$ or *Otud7b*$^{-/-}$*KrasLA2*, $n = 16$ at 16–23 weeks) and tumour numbers and size (**i**; *Otud7b*$^{+/+}$*KrasLA2*, $n = 10$ or *Otud7b*$^{-/-}$*KrasLA2*, $n = 12$ at 16 weeks) of the mice (mean±s.e.m., * * $P < 0.01$, Student's *t*-test). **j**, Kaplan–Meier survival curve of *Otud7b*$^{+/+}$*KrasLA2* and *Otud7b*$^{-/-}$*KrasLA2* mice at indicated age ($n = 20$ mice per group, * * * $P < 0.001$, log–rank test). **k**, Immunoblot of tissue lysates from *Otud7b*$^{+/+}$ or *Otud7b*$^{-/-}$ mice, with or without the *KrasLA2* transgene expression (three biological repeats). **l**, A model illustrating the roles of TRAF2/OTUD7B-controlled GβL polyubiquitination in

governing mTORC2 homeostasis. For uncropped gels, see Supplementary Fig. 1. For tumour data, see Source Data for **h**–**j**.